Title

The role of FXR and TGR5 in reversing and preventing progression of Western diet–induced hepatic steatosis, inflammation, and fibrosis in mice

Journal

Journal of Biological Chemistry, 298(11)

ISSN

0021-9258

Authors

Wang, Xiaoxin X
Xie, Cen
Libby, Andrew E
et al.

Publication Date

2022-11-01

DOI

10.1016/j.jbc.2022.102530

Peer reviewed

JBC RESEARCH ARTICLE

The role of FXR and TGR5 in reversing and preventing progression of Western diet–induced hepatic steatosis, inflammation, and fibrosis in mice

Received for publication, February 7, 2022, and in revised form, August 15, 2022 Published, Papers in Press, October 7, 2022,
https://doi.org/10.1016/j.jbc.2022.102530

Xiaoxin X. Wang[1,*], Cen Xie[2], Andrew E. Libby[1], Suman Ranjit[1], Jonathan Levi[3], Komuraiah Myakala[1], Kanchan Bhasin[1], Bryce A. Jones[4], David J. Orlicky[5], Shogo Takahashi[1], Alexander Dvornikov[6], David E. Kleiner[3], Stephen M. Hewitt[3], Luciano Adorini[7], Jeffrey B. Kopp[3], Kristopher W. Krausz[2], Avi Rosenberg[8], James L. McManaman[9], Charles E. Robertson[10], Diana Ir[10], Daniel N. Frank[10], Yuhuan Luo[10], Frank J. Gonzalez[2], Enrico Gratton[6], and Moshe Levi[1,*]

From the [1]Department of Biochemistry and Molecular & Cellular Biology, Georgetown University, Washington, District of Columbia, USA; [2]National Cancer Institute, and [3]National Institute of Diabetes and Digestive and Kidney Diseases, National Institutes of Health, Bethesda, Maryland, USA; [4]Department of Pharmacology and Physiology, Georgetown University, Washington, District of Columbia, USA; [5]Department of Pathology, University of Colorado AMC, Aurora, Colorado, USA; [6]Department of Biomedical Engineering, Laboratory for Fluorescence Dynamics, University of California at Irvine, Irvine, California, USA; [7]Intercept Pharmaceuticals, New York, New York, USA; [8]Department of Pathology, Johns Hopkins University, Baltimore, Maryland, USA; [9]The Integrated Physiology Programx, and [10]Department of Medicine, University of Colorado AMC, Aurora, Colorado, USA

Edited by Qi-Qun Tang

Nonalcoholic steatohepatitis (NASH) is the most common chronic liver disease in the US, partly due to the increasing incidence of metabolic syndrome, obesity, and type 2 diabetes. The roles of bile acids and their receptors, such as the nuclear receptor farnesoid X receptor (FXR) and the G protein-coupled receptor TGR5, on the development of NASH are not fully clear. C57BL/6J male mice fed a Western diet (WD) develop characteristics of NASH, allowing determination of the effects of FXR and TGR5 agonists on this disease. Here we show that the FXR-TGR5 dual agonist INT-767 prevents progression of WD-induced hepatic steatosis, inflammation, and fibrosis, as determined by histological and biochemical assays and novel label-free microscopy imaging techniques, including third harmonic generation, second harmonic generation, and fluorescence lifetime imaging microscopy. Furthermore, we show INT-767 decreases liver fatty acid synthesis and fatty acid and cholesterol uptake, as well as liver inflammation. INT-767 markedly changed bile acid composition in the liver and intestine, leading to notable decreases in the hydrophobicity index of bile acids, known to limit cholesterol and lipid absorption. In addition, INT-767 upregulated expression of liver p-AMPK, SIRT1, PGC-1α, and SIRT3, which are master regulators of mitochondrial function. Finally, we found INT-767 treatment reduced WD-induced dysbiosis of gut microbiota. Interestingly, the effects of INT-767 in attenuating NASH were absent in FXR-null mice, but still present in TGR5-null mice. Our findings support treatment and prevention protocols with the dual FXR-TGR5 agonist INT-767 arrest progression of WD-induced NASH in mice mediated by FXR-dependent, TGR5-independent mechanisms.

Nonalcoholic fatty liver disease (NAFLD) is one of the most common causes of liver disease in the United States, in part due to the increasing incidences of metabolic syndrome, obesity, and type 2 diabetes mellitus (1). About 20 percent of people with NAFLD develop nonalcoholic steatohepatitis (NASH) (2). The histological phenotype of NASH extends from steatosis to steatohepatitis, which can then progress to advanced fibrosis, cirrhosis, and hepatocellular carcinoma (1, 3). Recent human biopsy studies indicate that the transition from steatosis to steatohepatitis is a dynamic process, and the presence of fibrosis is the greatest prognostic value to predict the progression of NASH to cirrhosis and hepatocellular carcinoma (4).

Current clinical management of NASH is based on lifestyle intervention, including calorie-restricted diets and increased physical activity to promote weight loss (5). However, since weight loss is not always successful, additional surgical (6) and pharmacological (7) interventions are being explored. Bariatric surgery, including Roux-en-Y gastric bypass and vertical sleeve gastrectomy, were shown to result in significant weight loss and improvement of NASH (8). Several pharmacological interventions, including vitamin E, thiazolidinediones (PPAR-γ agonists), and the farnesoid X receptor (FXR) agonist obeticholic acid (OCA, 6α-ethyl-3α, 7α-dihydroxy-5-β-cholan-24-oic acid, INT-747) have shown beneficial effects in NASH, but no drug is currently approved for this indication (9–12). Importantly, OCA was also shown to improve fibrosis in NASH patients (12) and has recently completed the interim analysis of a pivotal phase 3 trial in NASH (12).

* For correspondence: Moshe Levi, Moshe.Levi@georgetown.edu; Xiaoxin X. Wang, Xiaoxin.Wang@georgetown.edu.

Interestingly, vertical sleeve gastrectomy results in significant alterations in bile acid metabolism and bile acid levels. For example, increases in serum cholic acid and tauroursodeoxycholic acid were found that could explain the positive effects of bile acid receptor activation (13). In mouse models of obesity, the beneficial effects of vertical sleeve gastrectomy were first shown to be FXR-dependent (14) and later also determined to be TGR5-dependent (15).

TGR5 is the G-protein-coupled bile acid receptor 1; a member of the rhodopsin-like subfamily of GPCRs. TGR5 is activated by bile acids, with the secondary bile acid lithocholic acid and its tauro-conjugate being the most potent endogenous agonists (16–18). The potent and selective TGR5 agonist (6α-ethyl-23(S)-methyl-3α, 7α, 12α-trihydroxy-5-β-cholan-24-oic acid), also known as INT-777, was shown to blunt diet-induced obesity and fatty liver (19) and was thereby hypothesized to play a role in preventing NASH.

We previously characterized the semi-synthetic bile acid derivative INT-767 (6α-ethyl-3α, 7α, 23-trihydroxy-24-nor-5-β-cholan-23 sulfate sodium salt) as the first agonist able to potently and selectively activate both FXR and TGR5 (20). INT-767 has three times higher potency than OCA to activate FXR, which makes it possible to deliver better efficacy at the same dose. Indeed, recently it has been reported that INT-767 can prevent and reverse diet-induced metabolic disorders such as NAFLD and atherosclerosis (21–27). In this study, we aim to further define the impact of INT-767 on the reversal and/or arrest of progression of Western diet (WD)-induced NASH, which is an increasingly relevant model to human disease.

The results indicate that the dual FXR-TGR5 agonist INT-767 can improve WD-induced liver injury and prevent progression to NASH. The effects of INT-767 reversing steatosis and fibrosis were mediated by FXR-dependent mechanisms, as shown by lack of efficacy in WD-fed *Fxr*-null mice, but not in *Tgr5*-null mice.

Results

INT-767 regulates expression of FXR and TGR5 target genes in liver and intestine

WD feeding did not significantly alter mRNA abundances of FXR target gene mRNAs *Cyp7a1*, *Cyp8b1*, *Shp*, or *Bsep* in mouse liver. As expected, treatment with the dual FXR/TGR5 agonist INT-767 markedly decreased *Cyp7a1* and *Cyp8b1* mRNA levels, while increasing *Shp* and *Bsep* mRNA levels, compared to nontreated controls (Fig. 1*A*). These results agree with the known ability of FXR activation to decrease hepatic bile acid levels by stimulating SHP-dependent suppression of CYP7A1-mediated bile acid synthesis and by increasing BSEP-dependent bile acid export (28, 29). In the ileum, INT-767 increased FXR targets *Fgf15* and *Shp* mRNAs (Fig. 1*B*), and *Gcg* mRNA encoded by a TGR5 target gene relative to untreated WD-fed mice (Fig. 1*C*). These results are in agreement with the known actions of FXR- and TGR5-mediated signaling in the ileum (19, 28, 29).

INT-767 treatment improves WD-induced NASH

WD-fed mice developed enlarged livers and showed liver injury with marked hepatocellular steatosis, liver inflammation, and fibrosis, typical of NASH (30). We undertook studies to determine whether INT-767 treatment could improve established liver pathology in WD-fed mice. Accordingly, following WD feeding for 3 months to allow induction of steatosis and hepatocellular liver injury (Fig. 2*A*), we added INT-767 to the WD and continued the experiment for another 3 months. Mice fed WD alone for 6 months had increased body and liver weights. Treatment with INT-767 for the last 3 months of the experimental period reversed the liver weight increase, without affecting body weight, food intake, or glucose homeostasis (Table 1). INT-767 also decreased serum aspartate transaminase (AST) and alanine transaminase (ALT) levels. While INT-767 did not alter fasting serum triglycerides, it lowered significantly the WD-induced increase in serum cholesterol.

Treatment of WD-fed mice with INT-767 improves liver triglyceride and cholesterol ester accumulation

Feeding mice the WD for 3 months resulted in steatosis with the start of inflammation (Fig. 2*A*). Treatment with INT-767 during the following 3 months reversed the WD-induced steatosis as determined by hematoxylin and eosin (H&E) staining (Fig. 2*B*) and perilipin-2 immunohistochemistry (Fig. 2*C*). The reversal of liver steatosis was also determined by fluorescence lifetime imaging microscopy (FLIM) and third harmonic generation (THG) (Fig. 2*D*). FLIM detected an increase in oxidized lipid species induced in WD-fed mice, which was prevented by INT-767 (Fig. 2*D*). INT-767 intervention significantly reduced the size of lipid droplets in WD-fed mice as revealed by THG histogram (Fig. 2*D*). This was revealed by the zoomed-in (90 μm) images showing small droplets and from the histogram (Fig. 2*D*).

Gas chromatography-mass spectroscopy analyses were used to further define how INT-767 intervention reversed hepatocellular steatosis. INT-767 intervention reduced liver triglycerides in WD-fed mice to control levels (Fig. 2*E*). The reduction in triglyceride levels was associated with significant alterations in hepatic triglyceride fatty acid composition (Fig. S1*A*), which resulted in a reduction in the fatty acid desaturation indexes (Fig. S1*B*), decreased ratios of unsaturated to saturated fatty acids (Fig. S1*C*), and increased polyunsaturated to monounsaturated fatty acids (Fig. S1*D*). Detailed analysis of lipogenic pathways in liver tissue demonstrated that INT-767 intervention significantly reduced mRNA levels of genes involved in regulation of de novo lipogenesis (*Srebp-1c*, *Chrebp-α*, and *Chrebp-β*), fatty acid desaturation (*Scd1*), and fatty acid uptake (*Cd36* and *Fabp1*) in both low-fat control diet (LF) and WD-fed mice (Fig. 2, *F* and *G*).

INT-767 intervention also reversed the WD-induced increases in hepatic cholesterol ester levels (Fig. 2*H*). This reversal was associated with significantly decreased expression of the oxidized LDL receptor, LOX-1 (Fig. 2*I*), which, together with CD36 (Fig. 2*G*), is a major mediator of cholesterol uptake. Notably, INT-767–mediated suppression of hepatic cholesterol

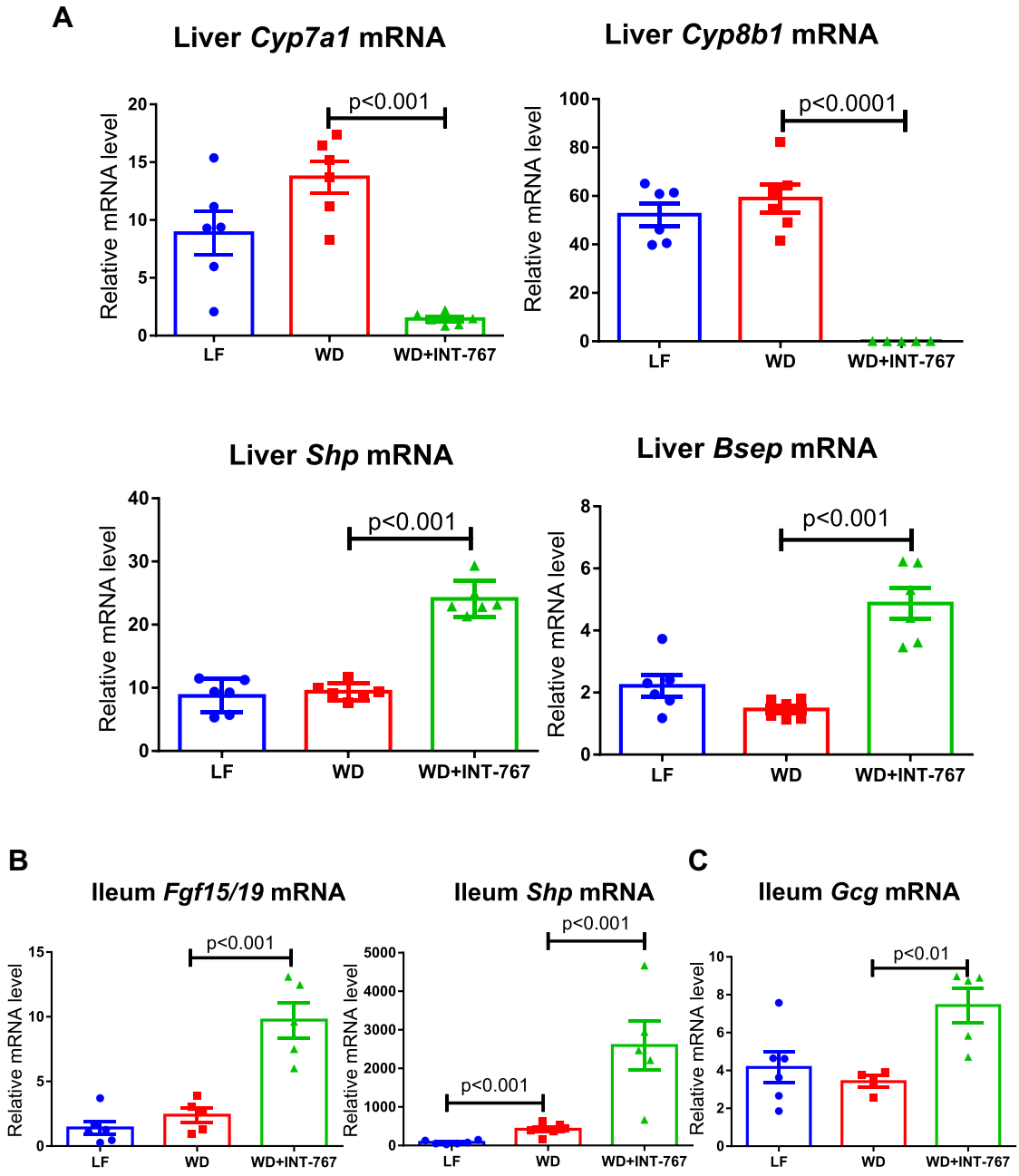

Figure 1. INT-767 regulates FXR target genes in the liver and regulates both FXR and TGR5 target genes in the ileum. *A*, INT-767 decreases liver *Cyp7a1* and *Cyp8b1* mRNA expression and increases liver *Shp* and *Bsep* mRNA expression. *B*, INT-767 increases the mRNA expression of FXR targets in the ileum: *Fgf15*, and *Shp* and *C*, TGR5 target genes in the ileum, *Gcg* mRNA. N = 6 mice. * = $p < 0.05$ WD *versus* LF; **$p < 0.05$ WD + INT-767 *versus* WD. FXR, farnesoid X receptor; LF, low-fat control diet; WD, Western diet.

levels subsequently upregulated the SREBP-2 pathway and downregulated LXR signaling as shown by increased SREBP-2-mediated cholesterol synthesis and decreased LXR-mediated expression of cholesterol efflux genes (Fig. 2*J*).

INT-767 improves WD-induced liver inflammation

Livers of mice fed WD exhibited evidence of inflammation as demonstrated by H&E staining (Table S1), CD3 immunohistochemistry (Fig. 3*A*), and increased mRNA levels of *Mcp-1*, *Tnfα*, and *Il-1β* (Fig. 3*B*). Treatment of WD-fed mice with INT-767 improved all of these inflammatory alterations.

The mouse liver injury scoring system (31) revealed that the WD drastically increased the percentage of hepatocytes showing macrosteatosis compared to those fed LF diet (Table S1). No mice fed the WD and treated with INT-767 reached this extent of macrosteatosis. However, all mice on WD demonstrated microsteatosis, in contrast to the LF diet-fed mice or WD-fed mice treated with INT-767. Coincidently with this increase in steatosis was a drastic increase in hepatic foci of inflammatory cells and lipogranulomas in WD-fed mice. These features were observed to a lesser extent in WD-fed mice treated with INT-767.

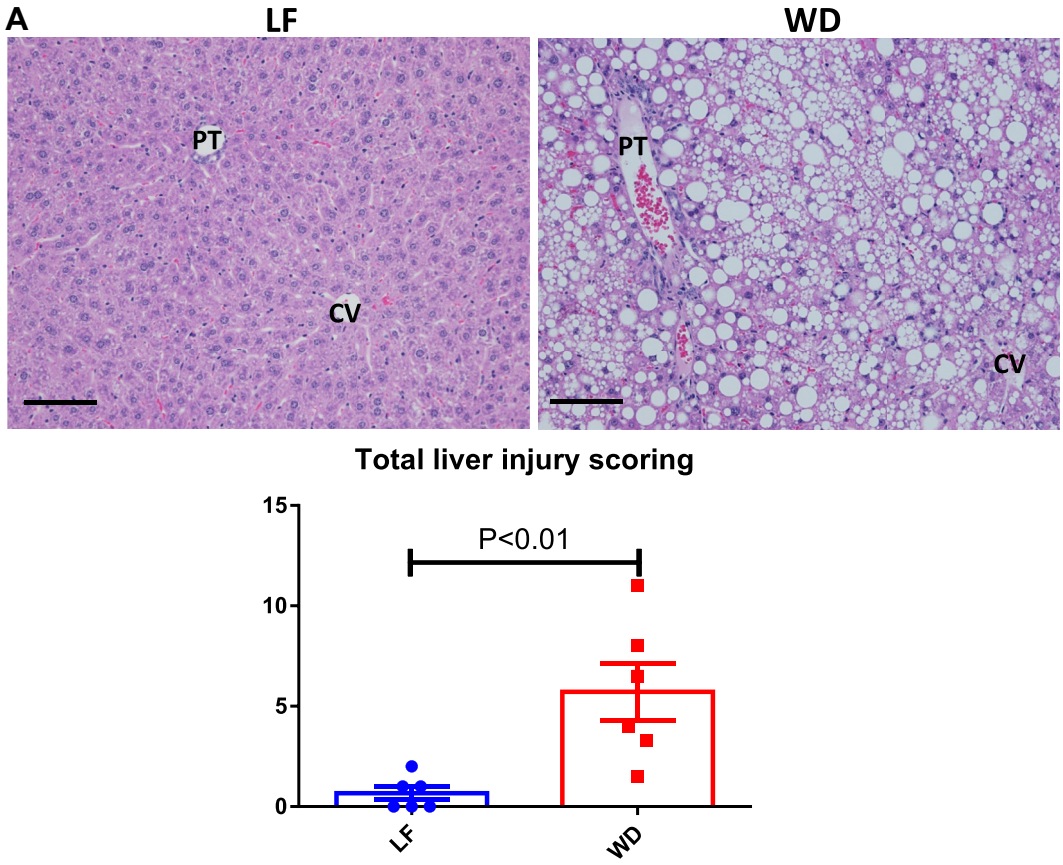

Figure 2. INT-767 prevents WD-induced steatosis, triglyceride, and cholesterol accumulation in the liver. *A*, steatosis as shown by H&E staining and liver injury scoring in mice on WD for 3 months compared to those on control low fat diet. *B–D*, steatosis as determined by (*B*) H&E stain, (*C*) perilipin-2 (PLIN2) immunohistochemistry for lipid droplets, (*D*) label-free imaging with fluorescence lifetime imaging microscopy (FLIM), and third harmonic generation (THG) microscopy. The *red areas* in FLIM images show the lipid droplets identified by the long lifetime in FLIM images and their boundaries can be seen in THG images. The histogram shows the changes in the droplet sizes calculated from FLIM data. The *p*-value on the histogram: $p < 0.0001$ LF *versus* WD and WD *versus* WD+INT-767. *E*, triglyceride content as determined by GC-MS. *F* and *G*, mediators of fatty acid synthesis; SREBP-1c, SCD1, ChREBP-α, and ChREBP-β with mRNA levels as determined by RT-qPCR. *G*, mediators of fatty acid uptake; *Cd36* and *Fabp1* with mRNA levels as determined by RT-qPCR. *H*, liver cholesterol ester content as determined by GC-MS. *I* and *J*, a mediator of cholesterol uptake, LOX-1, mediators of cholesterol synthesis, including SREBP-2 and HMG-CoA reductase, and mediator of cholesterol efflux including *ABCG5* and *ABCG8* mRNA levels are shown, as determined by RT-qPCR. N = 6 mice. Size bars = 100 microns. H&E, hematoxylin and eosin; LF, low-fat control diet; WD, Western diet.

INT-767 treatment arrests WD-induced liver fibrosis

WD-fed mice developed significant liver fibrosis and treatment with INT-767 nearly abrogated the development of fibrosis, which was assessed by Picro-Sirius Red staining of collagen fibers (Fig. 3*C*), label-free ratiometric two-photon excitation–second harmonic generation imaging (Fig. 3*D*), and collagen-I and collagen-III protein immunohistochemistry (Fig. 3*E*). The suppression of fibrosis following INT-767 intervention was associated with reduced expression of α-smooth muscle actin (*α-Sma*) and transforming growth factor (*Tgf*)-*β* (Fig. 3*F*), suggesting that arrest of fibrosis development may have been mediated by effects on hepatic stellate cell function (32).

INT-767 induces pronounced alterations in serum, liver, and intestine bile acid composition

Treatment with INT-767 blocked WD-induced increases in both total serum bile acid levels, and the serum levels of individual bile acids: TCA, T-α-MCA, T-β-MCA, T-DCA, T-HDCA, T-UDCA, and T-MDCA (Fig. *A*). INT-767 treatment of LF mice produced variable effects on individual bile acid serum levels but did not affect levels of total serum bile acids (Fig. 4*A*). In contrast to the WD effects on serum bile acids, total hepatic bile acid levels were not affected by WD feeding. Nevertheless, INT-767 treatment significantly suppressed total bile acid levels in LF- and WD-fed mice and produced variable effects on individual bile acid species, including TCA, T-α-MCA, T-β-MCA, T-DCA, T-UDCA, and T-MDCA (Fig. 4*B*). When expressed as relative composition, INT-767 treatment increased the percentage of more hydrophilic bile acids, such as T-β-MCA and T-α-MCA, whereas it markedly decreased the percentage of the less hydrophilic bile acid TCA in both LF- and WD-fed mice (Fig. 4*C*). As a result, there was a significant decrease in the hydrophobicity index of the liver bile acid composition, making it more hydrophilic (Fig. 4*C*). INT-767-mediated decreases in liver bile acid levels are consistent with, and most likely mediated by, a combination

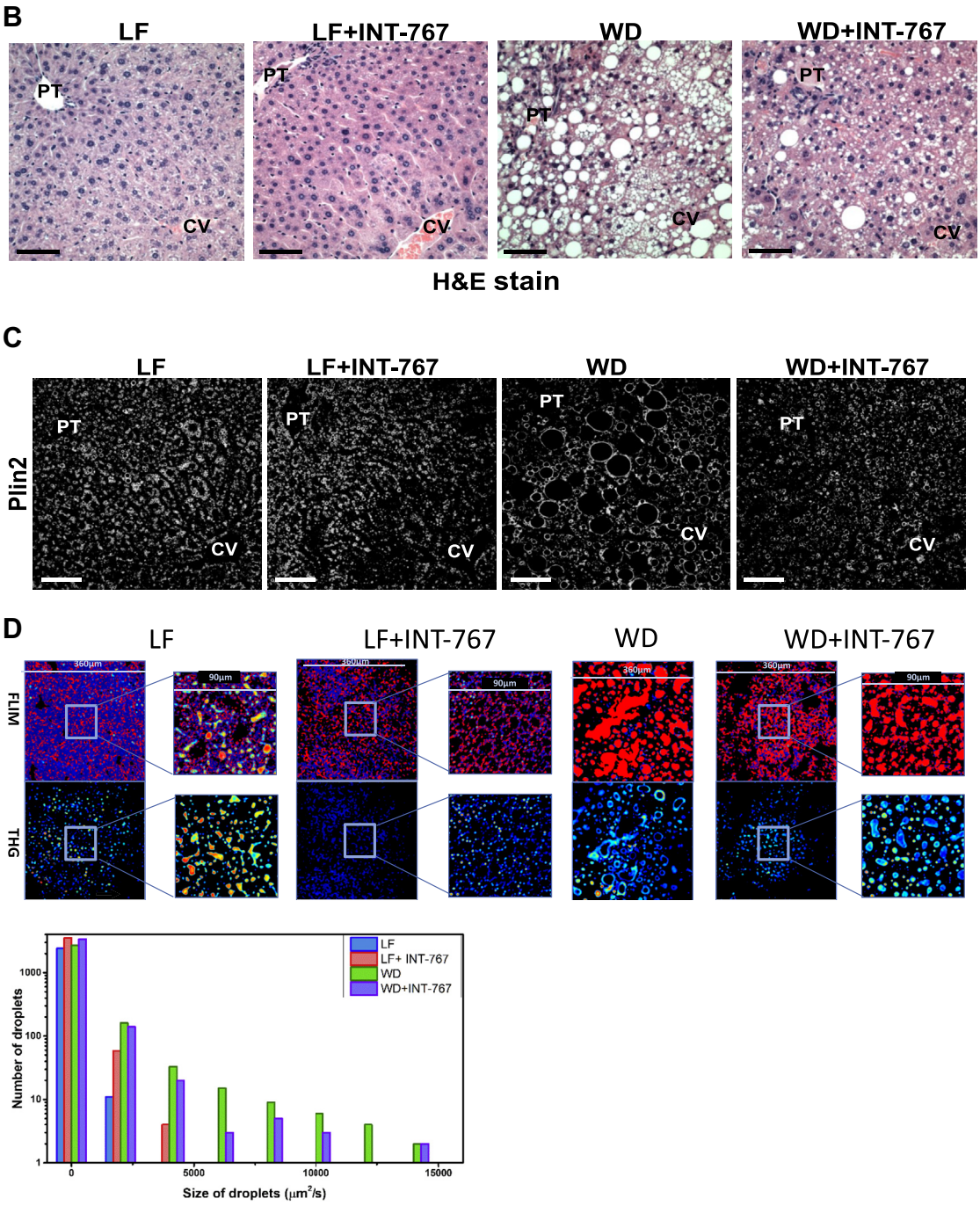

Figure 2. *(Continued).*

of decreased expression of liver bile acid synthesis enzymes (CYP7A1, CYP8B1) (Fig. 1*A*), increased expression of liver bile acid transporter for excretion (*Bsep*), decreased expression of liver bile acid transporters for reabsorption (*Ntcp*, *Oatp*), and increased expression of bile acid transporter for efflux to the blood circulation (*Ostβ*) (Fig. 4*D*).

Similar changes were observed in ileal bile acids with reduced levels in total bile acids or almost all individual bile acid species measured in the ileum of INT-767-treated mice, despite elevated expression of the apical transporter ASBT. We also found an increased percentage of hydrophilic bile acids, which contributed to the decreased hydrophobic index in the ileum from INT-767-treated groups (Fig. 4*E*). We did not find detectable amounts of lithocholic acid or its tauro-conjugate in the ileum or liver following INT-767 treatment.

As shown above, treatment with INT-767 caused a significant decrease in the hydrophobicity of liver and intestinal bile acid composition. In spite of increased *Npc1l1* mRNA expression (data not shown), decreased hydrophobicity of liver and intestinal bile acid composition will lead to decreased intestinal cholesterol absorption (33), therefore reducing systemic cholesterol and liver cholesterol levels.

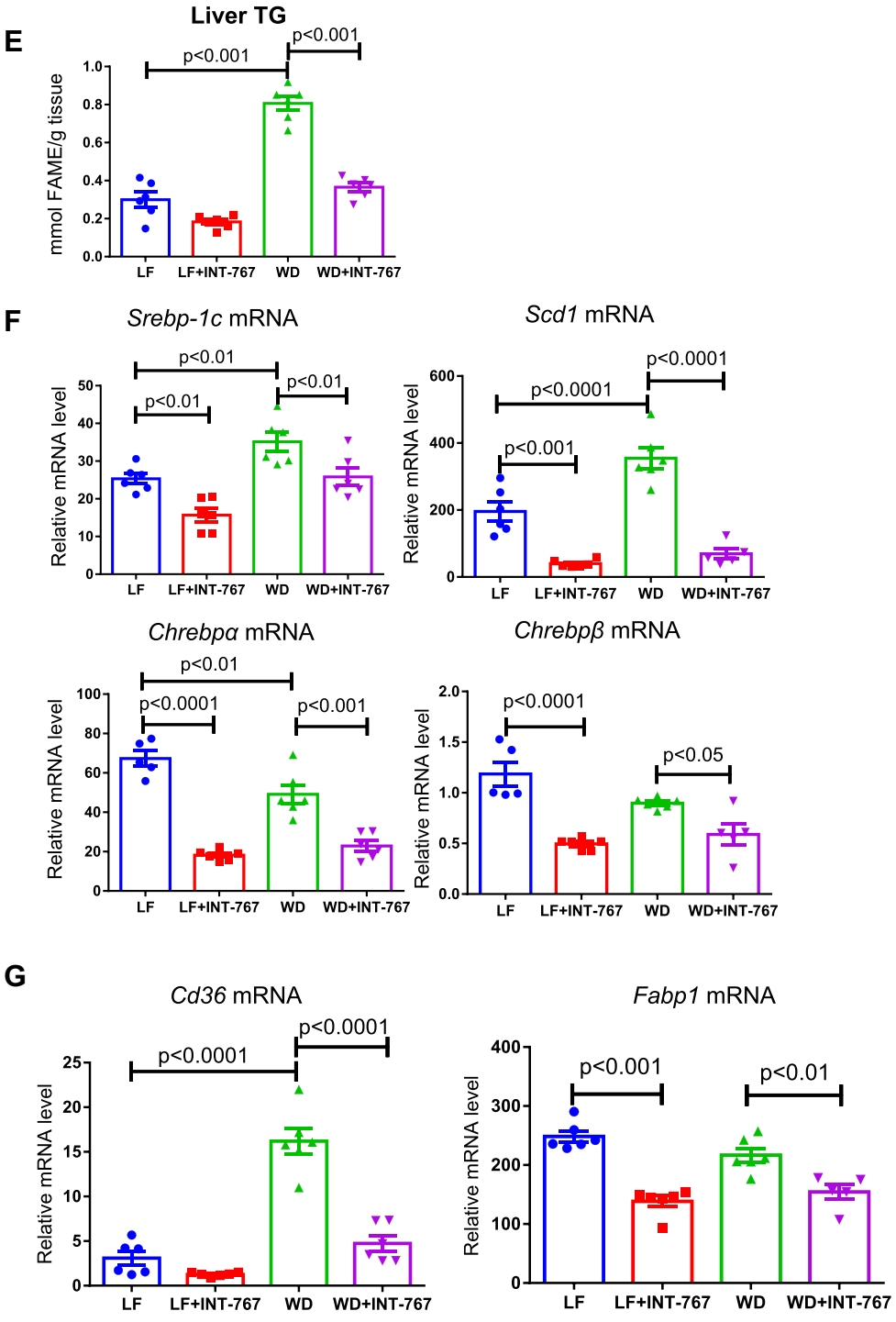

Figure 2. *(Continued).*

Treatment with INT-767 reverses WD-induced decreases in liver AMPK-SIRT1-PGC-1α-SIRT3 pathway

Mice fed WD had marked decreases in expression of SIRT1, PGC-1α, and SIRT3 (Fig. 5*A*). These alterations imply decreased mitochondrial biogenesis and mitochondrial function. We did not detect any alterations in mitochondrial number as determined by mitochondrial DNA/nuclear DNA ratio (Fig. 5*B*). However, WD induced a significant decrease in mitochondrial complex I activity (Fig. 5*C*). Treatment with INT-767 reversed the decreases in phospho-AMPK, SIRT1, PGC-1α, and SIRT3 (Fig. 5*A*) and significantly increased complex IV activity with a trend toward improving complex I activity (p = 0.07) (Fig. 5*C*).

INT-767-mediated inhibition of NAFLD and NASH development are FXR-dependent

Previous studies have shown that the FXR agonist OCA inhibits the development of NAFLD and NASH (10) and that

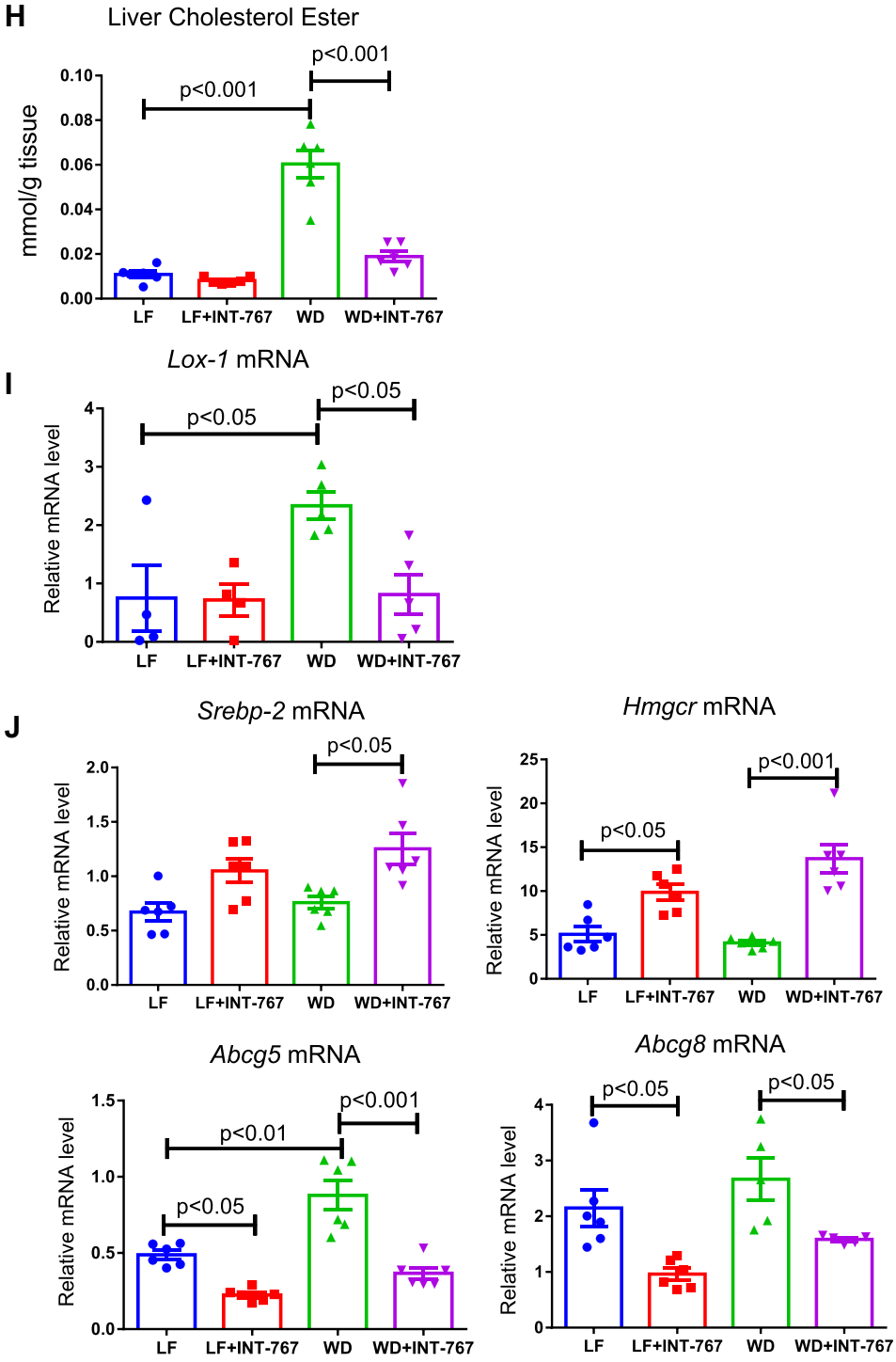

Figure 2. *(Continued).*

the TGR5 agonist INT-777 inhibits the development of NAFLD (19). To test whether the beneficial effects of INT-767 treatment are attributable to FXR or TGR5 agonism, *Fxr*-null mice were fed a WD and treated with either vehicle or INT-767.

The decrease in steatosis induced by INT-767 treatment was FXR-dependent, as determined by H&E staining (Fig. 6*A*) and liver triglyceride and cholesterol composition analysis (Fig. 6*B*). In addition, the beneficial effects of INT-767 preventing liver fibrosis were also dependent on FXR, as determined by Picro-Sirius Red staining (Fig. 6*C*), label-free imaging with second harmonic generation (SHG) microscopy (Fig. 6*D*), type I collagen and type III collagen immunohistochemistry (Fig. 6, *E* and *F*), quantitative collagen measurements by LC-MS/MS (Fig. 6*G*), and expression of pro-fibrotic *Tgf-β* and *α-Sma* mRNA levels (Fig. 6*H*).

Table 1
Metabolic parameters

Parameter	LF	LF + INT-767	WD	WD + INT-767
Body weight (g)	36.1 ± 1.06	33.7 ± 0.98	45.2 ± 0.65[a]	46.2 ± 2.32
Food intake (kcal/mouse/day)	11.7 ± 0.16	11.3 ± 0.06	19.0 ± 2.60[a]	19.2 ± 1.99
Liver weight/Body weight (%)	4.20 ± 0.10	5.95 ± 0.22[a]	8.24 ± 0.35[a]	6.71 ± 0.34[b]
Blood glucose (mg/dl)	247 ± 22	213 ± 20	228 ± 11	262 ± 19
AST (U/L)	25.3 ± 2.17	32.6 ± 4.72	56.0 ± 2.27[a]	39.6 ± 3.32[b]
ALT (U/L)	12.7 ± 1.05	13.1 ± 3.56	36.0 ± 0.40[a]	26.1 ± 1.37
Fasting serum cholesterol (mg/dl)	222 ± 11	N/A	438 ± 30[a]	294 ± 43[b]
Fasting serum triglycerides (mg/dl)	58 ± 5	N/A	70 ± 3	76 ± 7

Data are means ± SE (n = 6 mice in each group).
[a] $p < 0.05$ *versus* LF.
[b] $p < 0.05$ *versus* WD.

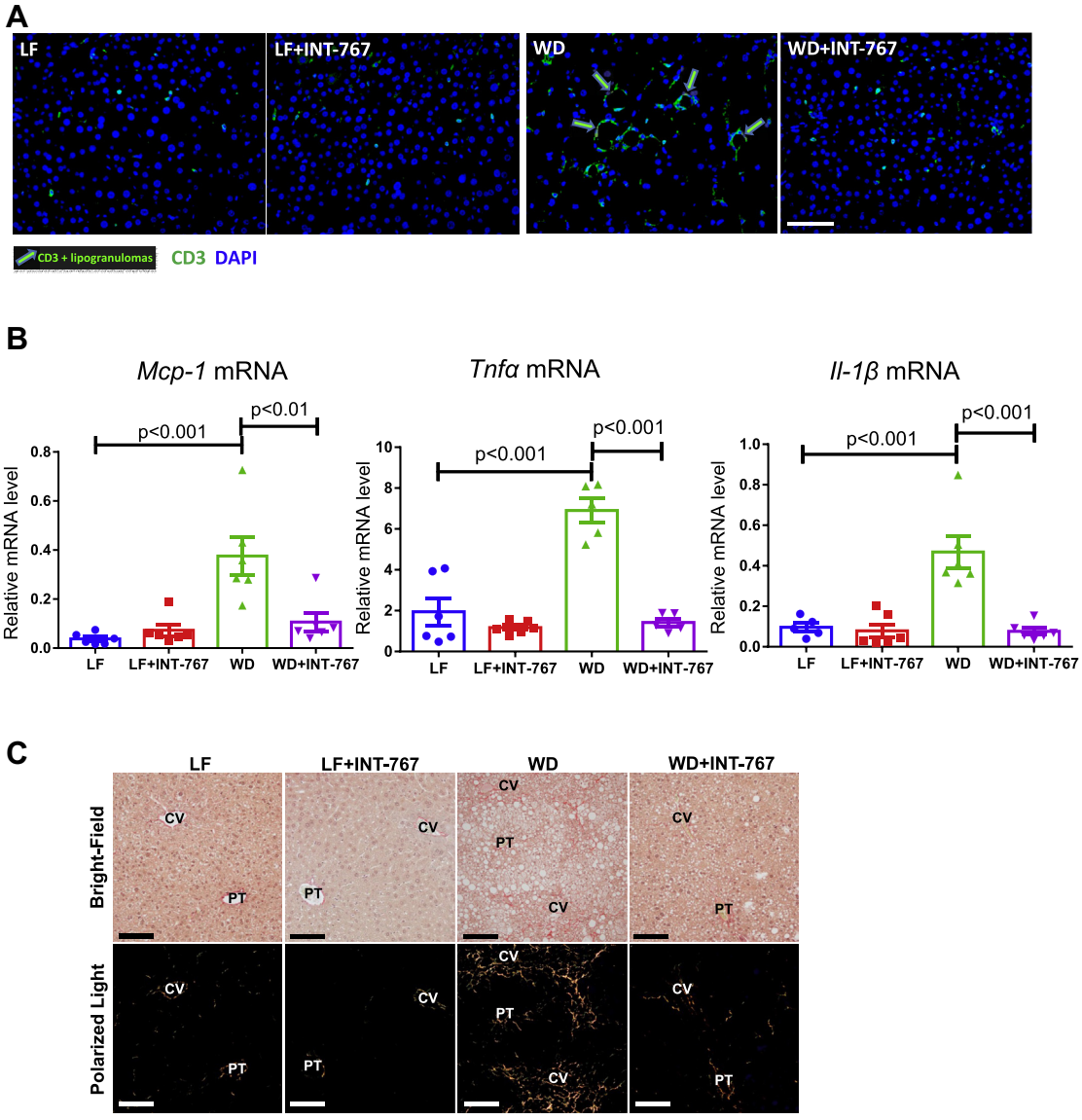

Figure 3. INT-767 prevents WD-induced inflammation and fibrosis in the liver. *A* and *B*, inflammation as determined by CD3 immunohistochemistry and MCP-1, TNF-α, and IL-1β mRNA levels; *C–E*, fibrosis as determined by (*C*) Picro-Sirius Red staining, (*D*) label-free imaging with ratiometric TPE-SHG microscopy, and (*E*) type I collagen and type III collagen immunohistochemistry. In (*D*), the ratio of fraction covered by SHG (*green*) to the area covered by autofluorescence (*red*) indicated by f_{green}/f_{red} shows the extent of fibrillar collagen accumulation and how INT-767 reverses the effect of WD. *F*, INT-767 decreased TGF-β and α-SMA mRNA levels. N = 6 mice. *$p < 0.05$ WD *versus* LF; **$p < 0.05$ WD + INT-767 *versus* WD. Size bars = 100 microns. LF, low-fat control diet; SHG, second harmonic generation; TPE, two-photon excitation; WD, Western diet.

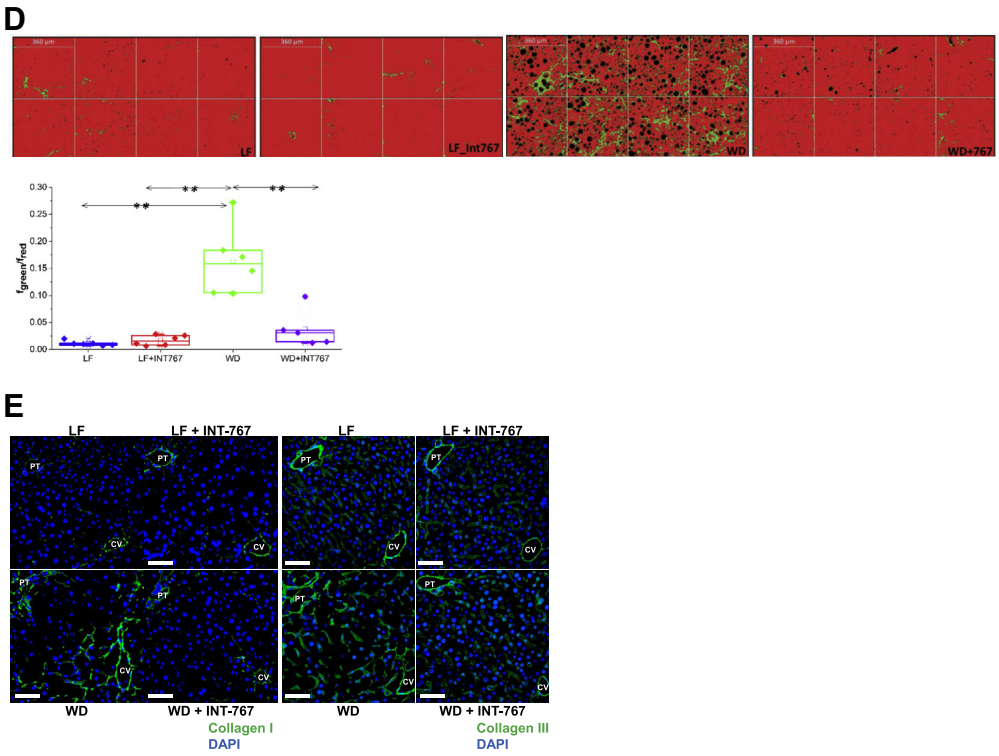

Figure 3. *(Continued).*

Likewise, although treatment of WD-fed mice with INT-767 increased p-AMPK, PGC-1α, SIRT3, and MnSOD, these effects were not observed in *Fxr*-null mice treated with INT-767 (Fig. 6*I*). Furthermore, treatment with the FXR agonist OCA (INT-747), but not the TGR5 agonist INT-777, increased *Pgc-1α* and *Sirt3* in the livers of WD-fed mice (Fig. 6*J*).

INT-767-mediated inhibition of NAFLD and NASH development are TGR5-independent

To test whether the beneficial effects of INT-767 treatment are also dependent on TGR5 agonism, we fed *Tgr5*-null mice a WD and treated them with either vehicle or INT-767. TGR5-null mice showed no significant difference in steatosis and liver fibrosis from wild-type mice on WD. However, to our surprise, INT-767 treatment still resolved the steatosis and fibrosis in the WD-fed NASH model in *Tgr5*-null mice (Fig. 7, *A* and *B*). To clarify the contribution of TGR5 agonism, we compared INT-767 with other two agonists, FXR specific INT-747 and TGR5 specific INT-777 in WD-induced NASH development. As expected, both INT-747 and INT-767 were beneficial in controlling liver injury and liver fibrosis, although INT-767 appeared to show better protection than INT-747 (Fig. 7, *C* and *D*). On the other hand, INT-777 treatment failed to decrease the liver injury and liver fibrosis, indicating that a TGR5 agonism alone is not sufficient in this NASH model (Fig. 7, *C* and *D*). Pathak *et al.* (27) reported that FXR can induce ileal TGR5. However, we did not find in our model that INT-767 can increase *Tgr5* expression in the ileum, or FXR deficiency can lower ileal *Tgr5* (Fig. S2).

INT-767 modifies gut microbiota

To understand the role of gut microbiota in this NASH model, bacterial communities inhabiting the cecum and colon

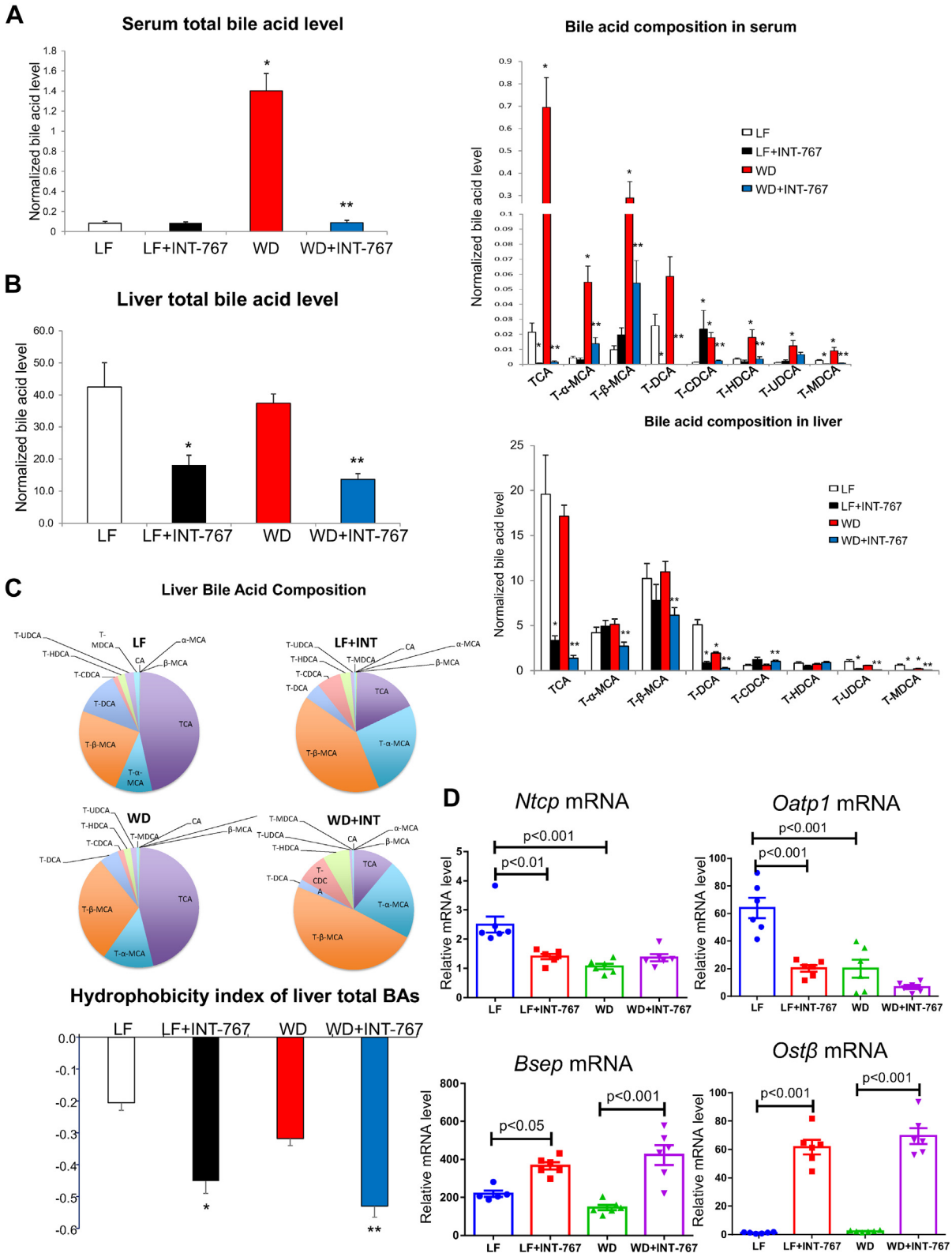

Figure 4. INT-767 regulates bile acid composition of serum, liver, and ileum. *A*, WD induced significant increases in serum total bile acids TCA, T-α-MCA, T-β-MCA, TDCA, T-HDCA, T-UDCA, and T-MDCA levels. Treatment with INT-767 prevented these increases and also resulted in significant decreases in serum TCA, T-α-MCA, T-β-MCA, TDCA, T-CDCA, T-HCDA, and T-MCDA levels. *B*, treatment of WD-fed mice with INT-767 also resulted in significant alterations in liver total bile acids and individual bile acid species including TCA, T-α-MCA, T-β-MCA, T-DCA, T-UDCA, and T-MDCA. *C*, when expressed as relative composition as shown in the pie chart, treatment with INT-767 increased the relative level of T-β-MCA and T-α-MCA but decreased that of TCA content. These changes resulted in a major decrease in the hydrophobicity index of the liver bile acid composition. *D*, treatment with INT-767 increased expression of liver bile salt export pump (BSEP), decreased expression of liver bile acid reabsorption transporters (NTCP, OATP) and increased expression of bile acid efflux transporters to the blood circulation (OSTβ). *E*, treatment of WD mice with INT-767 resulted in significant alterations in ileal total bile acids and in ileal individual bile acid

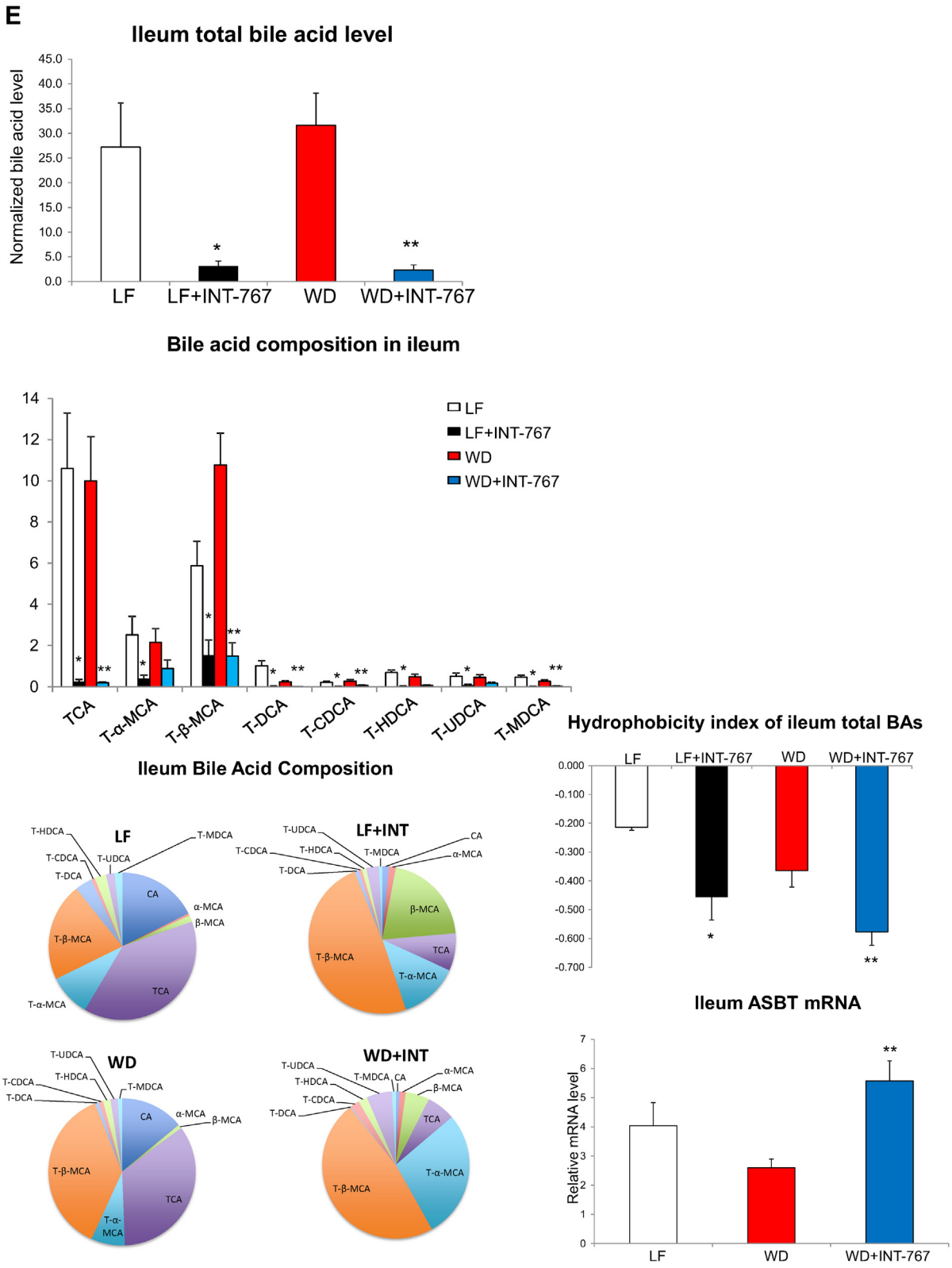

Figure 4. *(Continued).*

species. The pie chart for ileum bile acid composition showed the decreased TCA and increased T-β-MCA and T-α-MCA in INT-767 treated mice, which contributed to the decreased hydrophobicity index. N = 6 mice. *$p < 0.05$ WD *versus* LF; **$p < 0.05$ WD + INT-767 *versus* WD. LF, low-fat control diet; WD, Western diet.

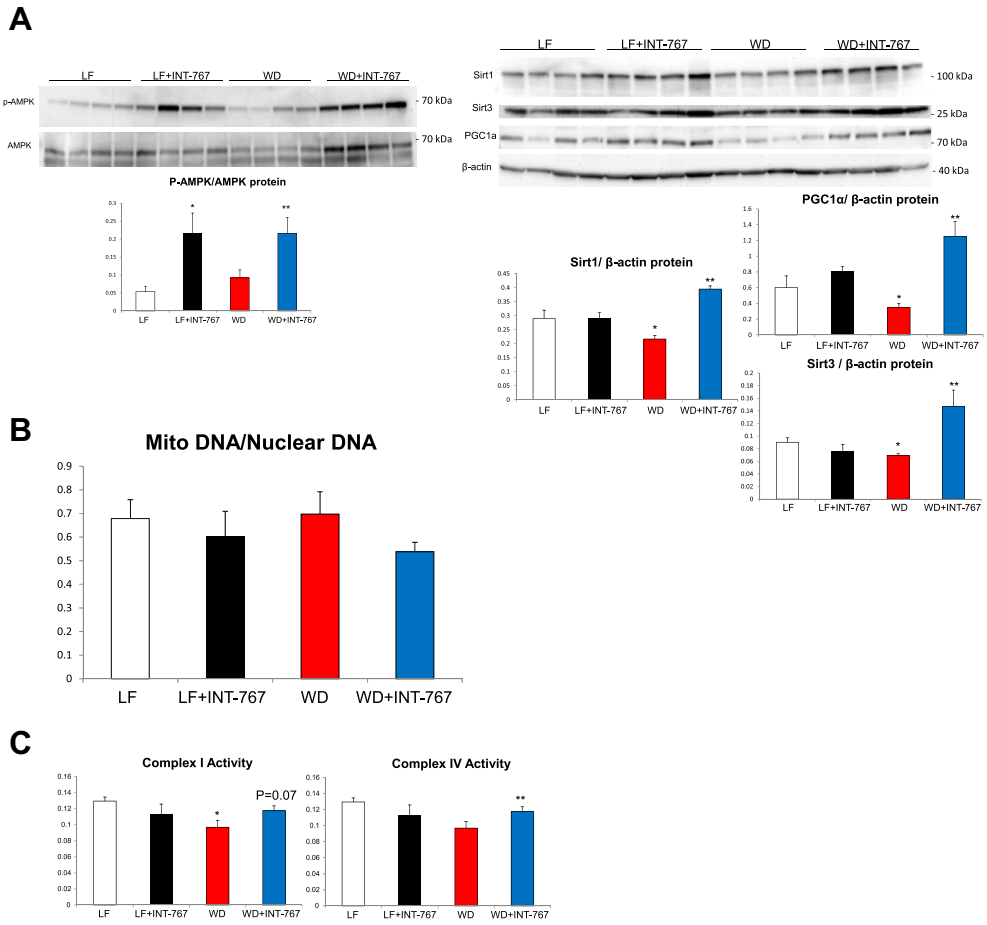

Figure 5. INT-767 increased mitochondrial function. *A*, p-AMPK, SIRT1, PGC-1α, and SIRT3 protein levels were determined by Western blotting and normalization to β-actin. *B*, mitochondrial DNA/nuclear DNA ratio. *C*, complex I and complex IV activity were determined by kits from MitoSciences/Abcam. N = 6 mice. *$p < 0.05$ WD *versus* LF; **$p < 0.05$ WD + INT-767 *versus* WD. LF, low-fat control diet; WD, Western diet.

were profiled in all treatment groups by 16S rRNA gene sequencing. Both the overall composition (Fig. 8*A*) and biodiversity (Fig. S3*A*) of the microbiota were affected to varying degrees by diet, FXR genotype, and INT-767 treatment. Based on nonparametric multivariate analysis of variance tests of overall community composition (*i.e.*, beta-diversity), the colonic microbiota ($p < 0.00001$) were altered to a greater extent by these factors than were cecal microbiota ($p = 0.10$). Furthermore, diet (LF *versus* WD; $p = 0.0050$) and FXR genotype ($p < 0.00001$) were more significantly associated with colonic microbiota composition than was INT-767 treatment ($p = 0.38$; Fig. 8*A*). Nonetheless, pairwise comparisons of both WT WD *versus* WT WD+INT767 ($p = 0.0066$) and FXR KO WD *versus* FXR KO WD+INT767 ($p = 0.0079$) indicated that INT-767 treatment induced significant shifts in colon microbiota of WD-fed animals, regardless of FXR genotype. However, WT LF and WT WD+INT767 treatment groups also differed in microbiota composition ($p = 0.028$), indicating that INT-767 did not completely reverse WD-induced dysbiosis.

In terms of individual operational taxonomic units, multiple phylum- and genus-level taxa were altered in the colonic microbiota of WD-fed WT animals, compared with LF-fed WT animals (Figs. 8*B* and S3*B*). The most notable change was in the phylum Bacteroidetes (Fig. 8*B*), which was greatly increased in WD-fed animals (27.8% *versus* 9.7% relative abundance in WT WD *versus* WT LF groups; $p = 0.022$). These changes were due primarily to shifts in the S24-7 group of Bacteroidetes (23.0% *versus* 9.6%; $p = 0.0043$). Conversely, WD-feeding was associated with slightly diminished Firmicutes (69.2% *versus* 75.8%; $p = 0.041$), including genera such as *Allobaculum* (1.2% *versus* 4.2%; $p = 0.0022$) and *Lactobacillus* (0.37% *versus* 12.8%; $p = 0.04$). However, some groups of Firmicutes, such as *Roseburia* (0.71% *versus* 0.16%; $p = 0.0022$) were increased in abundance in WD-fed animals. Treatment of WT WD mice with INT-767 (*i.e.*, WT WD+INT767) reversed most of these effects (Figs. 8*B* and S3*B*), resulting in Bacteroidetes and Firmicutes abundances that were more similar to WT-LF mice. In contrast, INT-767 treatment of FXT KO WD animals (*i.e.*, FXR KO WD+INT-767) exaggerated the effects of WD feeding, as evidenced by elevated Bacteroidetes (48.3% *versus* 30.1% for FXR KO WD+INT-767 *versus* FXR KO WD; $p = 0.016$) and diminished Firmicutes (46.8% *versus* 50.7%; $p = 0.056$). These results are consistent with the phenotypic and molecular data presented above, which indicate that FXR is required for INT-767 activity.

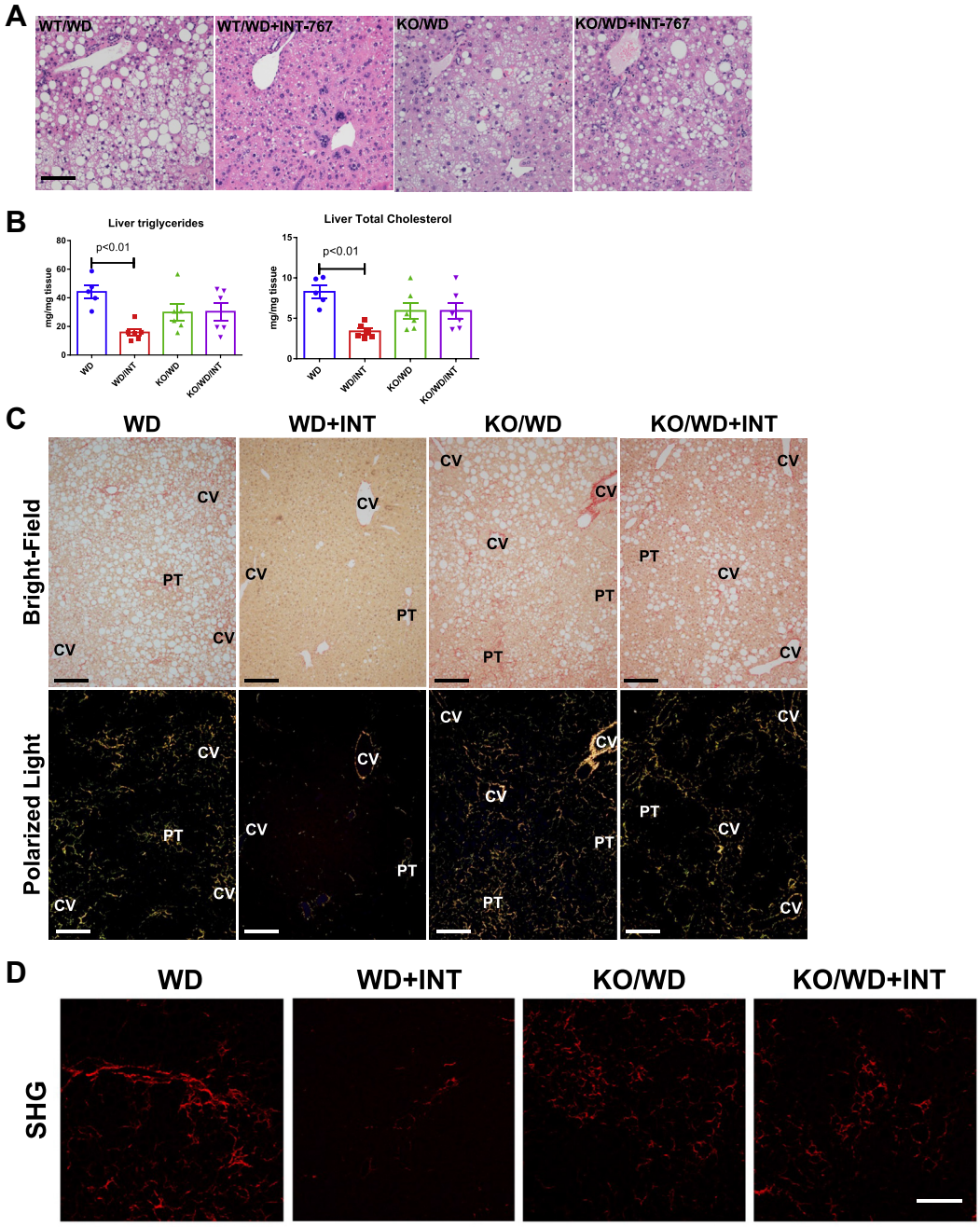

Figure 6. The effects of INT-767 on NASH are FXR-dependent. *A* and *B*, steatosis as determined by H&E staining, liver triglyceride, and cholesterol content; *C–H*, fibrosis as determined by (*C*) Picro-Sirius Red staining, (*D*) label-free imaging with SHG, (*E*) collagen I, and (*F*) collagen III immunohistochemistry, (*G*) quantitative measurement of collagen 1a1, collagen 1a2, and collagen 3a1 by LC-MS/MS, and (*H*) *TGF-β* and *α-SMA* mRNA levels. Size bars = 100 microns. *I*, the effects of INT-767 to stimulate p-AMPK, PGC-1α, SIRT3, and SOD2 protein are FXR-dependent. INT-767 stimulates p-AMPK, PGC-1α, SIRT3, and SOD2 protein in wildtype mice fed a WD but not in *Fxr-null* mice fed a WD. *J*, treatment of WD-fed mice with the FXR agonist OCA (INT-747) but not the TGR5 agonist INT-777 induces upregulation of PGC-1α and SIRT3 mRNA. N = 6 mice. *$p < 0.05$ WD *versus* LF; **$p < 0.05$ WD + INT-767 *versus* WD. Size bars = 100 microns. FXR, farnesoid X receptor; H&E, hematoxylin and eosin; LF, low-fat control diet; NASH, nonalcoholic steatohepatitis; WD, Western diet.

We next examined the relationships between intestinal bile acid pools and gut microbiota, in the WT-LF, WT-WD, and WT-WD-INT767 treatment groups, by systematically performing Spearman rank correlation tests between the abundances of bile acid species and microbial taxa. Distinct patterns of association were observed in this analysis (Fig. 8*C*), with the colon exhibiting more significant associations than the cecum. Within the colon, several groups of the phylum Firmicutes, most notably *Ruminococcaceae* and *Coprococcus*, were significantly negatively correlated with unconjugated primary and secondary bile acids. In contrast, members of the phylum Bacteroidetes, such as the *Bacteroides*, *Parabacteroides*, and S24-7, were positively correlated with these same unconjugated bile acids.

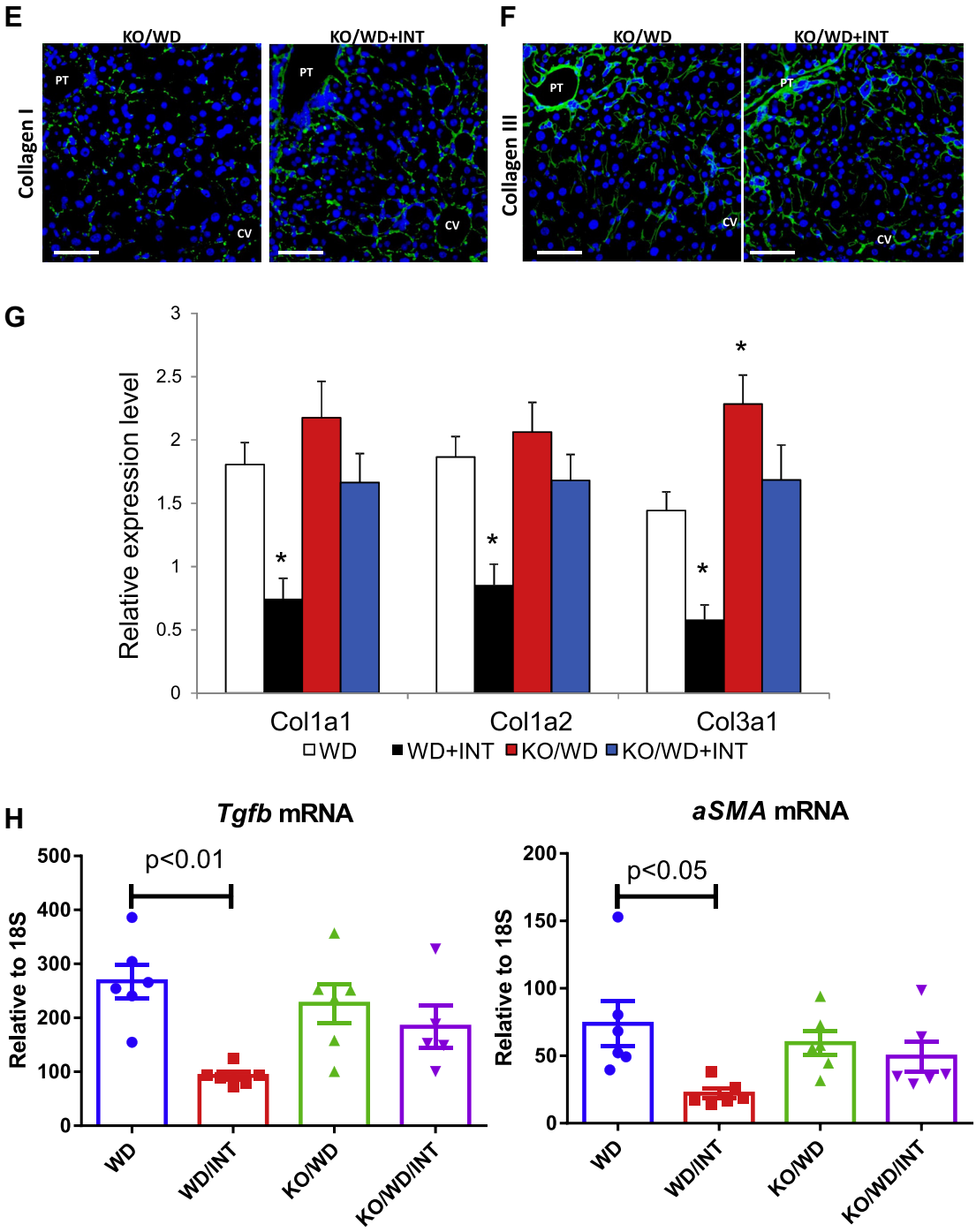

Figure 6. *(Continued).*

INT-767 treatment reduces methionine and choline–deficient diet–induced liver steatosis but not fibrosis

To further investigate how INT-767 exerts its anti-fibrosis role, we used another diet, methionine and choline–deficient diet (MCD), to generate NASH in mice (30). MCD-induced liver fibrosis does not seem to depend on liver steatosis (34). After 12-weeks on MCD diet, severe fibrosis developed in the liver as assessed by Picro-Sirius Red staining (Fig. 9*B*). However, although INT-767 significantly reduced steatosis (Fig. 9*A*), MCD-induced hepatic fibrosis was not affected by INT-767 treatment (Fig. 9*B*).

FXR and TGR5 proteins are expressed in liver biopsy tissue obtained from donors with no liver disease and subjects with NAFLD and NASH

H&E and Masson's trichrome stains showed clear evidence of steatosis and fibrosis in liver sections from subjects with NAFLD and NASH, which are lacking from donors without liver disease (Fig. S4*A*). SHG microscopy, which images fibrillary collagens in a label-free manner, further documented marked differences in the degree of fibrosis between diseased and nondiseased human liver (Fig. S4*A*). FXR and TGR5 were detected in liver sections from both NASH and nondiseased

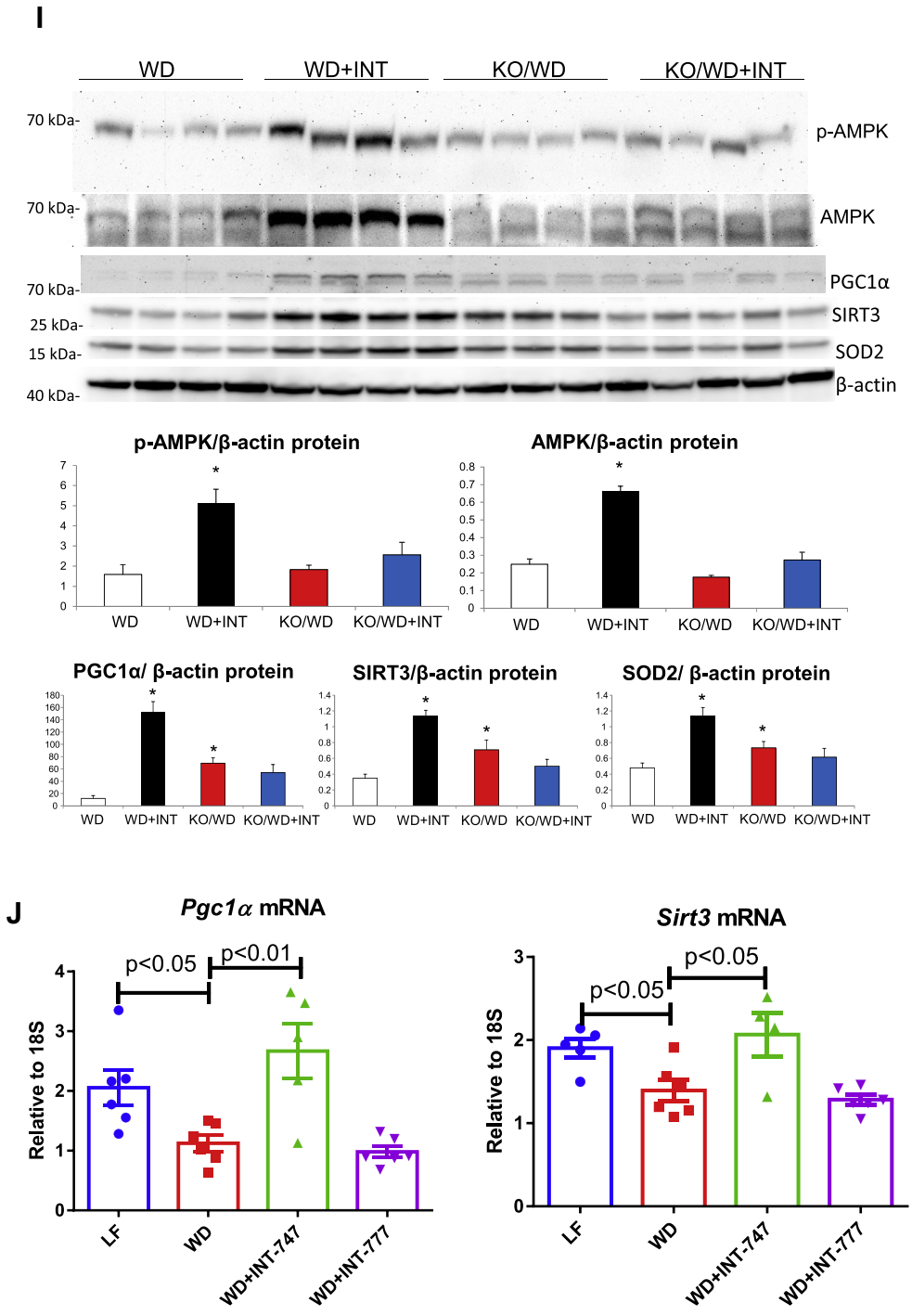

Figure 6. *(Continued).*

donor patients by immunohistochemistry. FXR was predominantly expressed in hepatocyte and cholangiocyte nuclei in sections from NASH patients and showed a significant increase in staining intensities compared to nondiseased controls (p = 0.004). Membranous TGR5 staining was selectively localized to cholangiocytes in the bile ducts from both nondiseased and NASH patients. The significantly increased number of TGR5-positive cholangiocytes in NASH liver sections compared to controls (p = 0.0012) reflects ductular reaction (Fig. S4*B*).

Discussion

The prevalence of NASH is increasing worldwide in part due to the increased prevalence of obesity and diabetes. There are currently no pharmacological treatments for NASH. Here we report that C57BL/6J male mice fed a WD composed of milk fat, sucrose, and cholesterol, as used in atherosclerosis models, develop NASH features, including hepatic steatosis, inflammation, and fibrosis, as determined by classical histological stains and biochemical assays as well as novel and label-free microscopy imaging techniques including THG, SHG, and

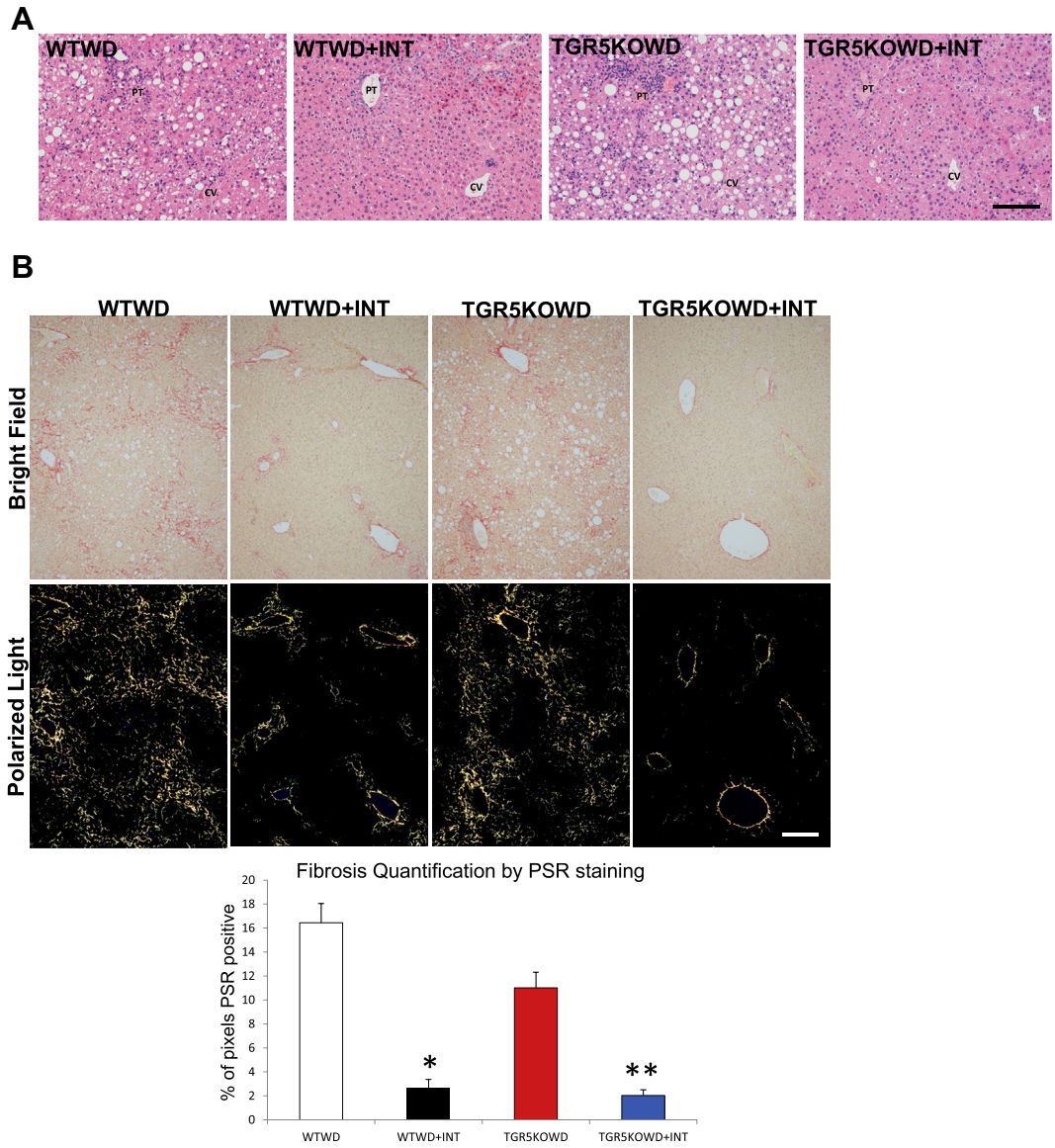

Figure 7. The effects of INT-767 on NASH are TGR5-independent. *A* and *B*, steatosis as determined by H&E staining (*A*) and fibrosis as determined by Picro-Sirius Red staining with subsequent quantification (*B*). Only groups of wild-type WD (WTWD), wild-type WD+ INT-767 (WTWD + INT), TGR5KO WD, and TGR5KO WD+INT-767 in the study were compared. *C* and *D*, steatosis as determined by H&E staining with quantification of liver total injury (*C*) and fibrosis as determined by Picro-Sirius Red staining with quantification (*D*). Only groups of wild-type WD [reuse of WTWD images of H&E (panel *A*) and polarized Picro-Sirius Red staining (panel *B*)], wild-type WD+ INT-747, wild-type WD+ INT-767 [reuse of WTWD + INT images of H&E (panel *A*), and polarized Picro-Sirius Red staining (panel *B*)], and wild-type WD+ INT-777 in the study were compared. N = 6 mice. *$p < 0.05$ *versus* WTWD; **$p < 0.05$ *versus* TGR5KOWD. Size bars = 100 microns. H&E, hematoxylin and eosin; NASH, nonalcoholic steatohepatitis; WD, Western diet.

FLIM. In this study, we found that the FXR-TGR5 dual agonist INT-767 prevents the progression of WD-induced liver injury. This effect is dependent on FXR but not TGR5.

Although INT-767 was found to improve liver steatosis in different models, whether it can also attenuate liver fibrosis, a hallmark of NASH, has not been fully explored (21, 26, 27, 35). In this study, we employed different methods to study the antifibrotic effects of INT-767 treatment in a NASH model. Conventional Picro-Sirius Red staining showed decreased fibrillar collagen deposits in the treated liver, and immunohistochemistry confirmed a reduced accumulation of collagen I and III after INT-767 treatment. Furthermore, we used mass spectrometry to quantify individual collagen subunits and found decreased expression of collagen 1α1, collagen 1α2, and collagen 3α1 chains in the treated liver. Finally, we used a multiphoton microscope equipped with Deep Imaging *via* Enhanced-Photon Recovery (DIVER) detector for SHG imaging that can distinguish fibrillary collagen accumulation even in the early stages of fibrosis, unlike standard histological analysis (36–38). The SHG imaging clearly showed decreased fibrosis in INT-767-treated mice. The antifibrotic role of INT-767 is remarkably similar to the beneficial effects induced by OCA treatment in animal models (39, 40) and patients with NASH (10, 12). Recently, in a rabbit model of high fat diet–induced NASH, INT-767 was shown to prevent liver fibrosis (24). Using *ob/ob* mice fed the high fat with trans fat,

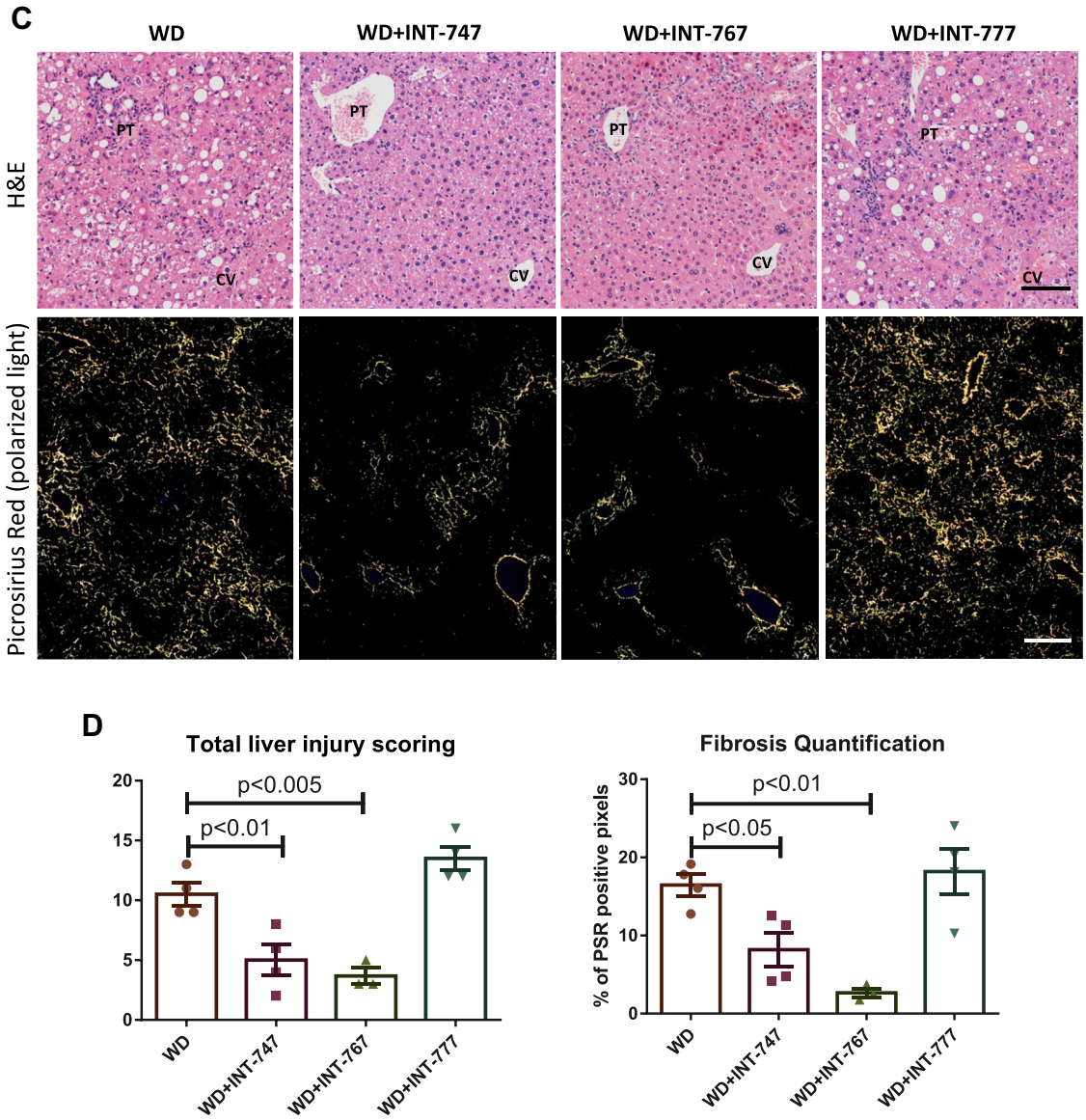

Figure 7. *(Continued).*

cholesterol, and fructose, INT-767 could also reverse NASH (25). Consistent with these findings, our study confirmed that INT-767 treatment can improve liver fibrosis in a mouse model of WD-induced NASH. Since INT-767 treatment was started after 3 months on WD, when liver injury was already established, our data indicate that INT-767 can arrest the progression of liver fibrosis in NASH thus indicating its therapeutic potential.

In terms of the mechanism by which INT-767 exerts its antifibrotic effects, it is conceivable that the agonism of either FXR or TGR5 could make contributions and if so, the dual agonism may carry an advantage to singular agonism. In the diet-induced obesity model, steatosis is believed to be the first hit for fibrosis which appears later in disease progression (41). Both FXR and TGR5 are found to be involved in improving liver steatosis (19, 42–45). However, to our surprise, we observed that improvement of NASH by INT-767 depends on activation of FXR rather than TGR5. Pathak *et al.* (27) reported an FXR-dependent but TGR5-independent mechanism for INT-767 based on the TGR5 activation by FXR. In contrast, our data showed that FXR activation could not induce TGR5 expression. However, we cannot rule out the possibility that FXR can still induce GLP-1 secretion in the absence of TGR5 (27).

To further clarify the mechanism, we compared the different agonists in the NASH model. We found that the TGR5-specific agonist INT-777 failed to show the protective effects in the liver injury and liver fibrosis, whereas both INT-767- and FXR-specific agonist OCA significantly reduced the liver injury and fibrosis. These results suggest that TGR5 agonism alone is not enough to treat the NASH, although it can reduce hepatic steatosis in other reports (19) and that FXR activation plays a major role in INT-767 to treat the NASH.

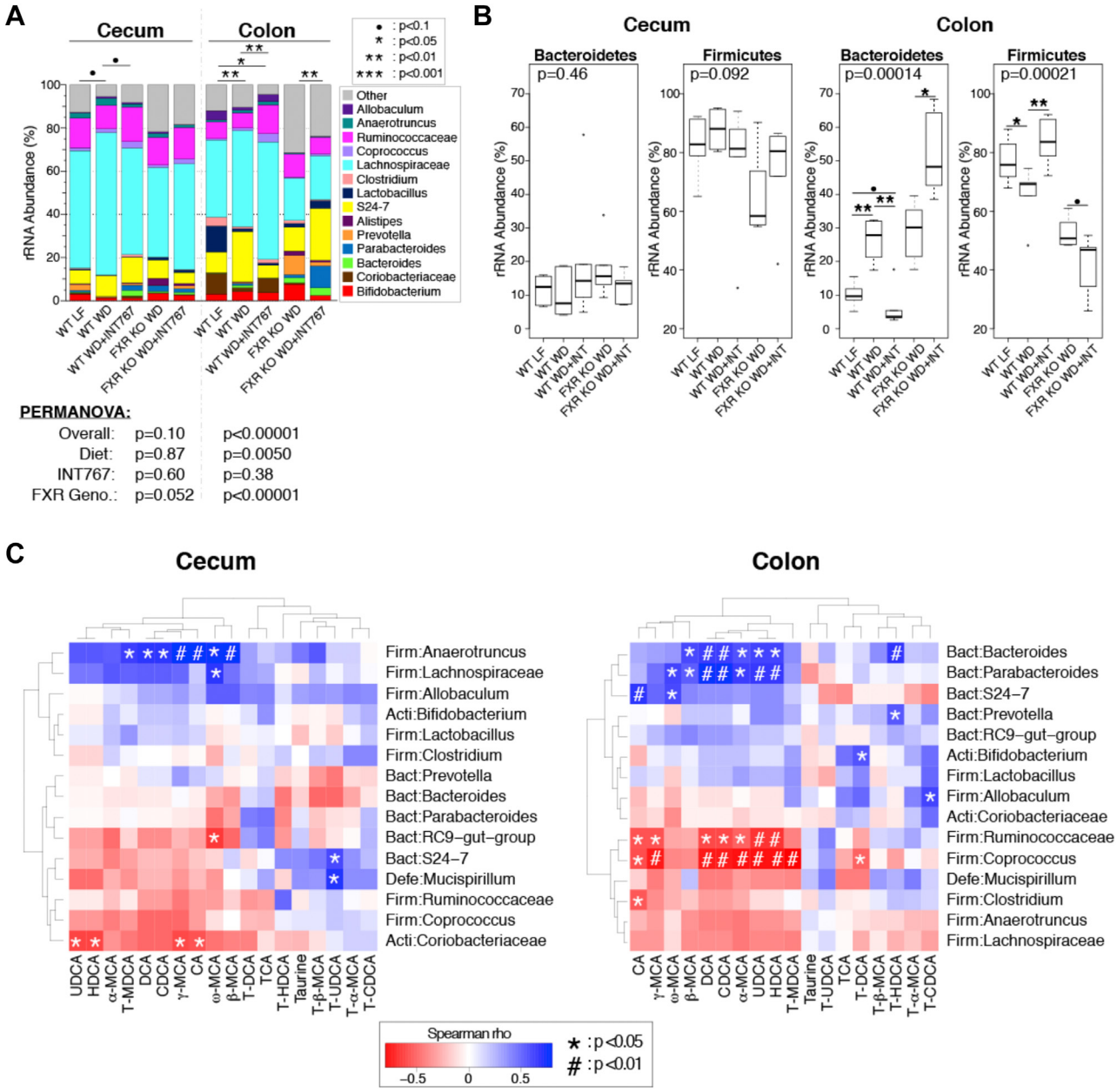

Figure 8. WD and INT-767 modulate the microbiota. *A*, distribution of bacterial genera in cecal and colon contents. Results of permutation-based multiple analysis of variance (PERMANOVA) tests for pairwise comparisons between treatment groups are shown by symbols above bar charts. PERMANOVA tests across all treatment groups are summarized below bar charts: "Overall" shows the *p*-value for tests across all five treatment groups, while "Diet", "INT767", and "FXR geno" summarize the *p*-values for multiple-factor PERMANOVA tests. •$p < 0.1$; *$p < 0.05$; **$p < 0.01$. *B*, summary of relative abundances of the key intestinal phyla, Bacteroidetes, and Firmicutes, across treatment groups. •$p < 0.1$; *$p < 0.05$; **$p < 0.01$. *C*, heatmaps displaying Spearman rho correlation coefficients for pairwise comparisons of cecal bile acid species *versus* cecal or colonic microbial taxa (top 15 most abundant genus-level taxa). Genus-level taxon names are preceded by abbreviated phylum names: Acti: Actinobacteria, Bact: Bacteroidetes, Firm: Firmicutes. *$p < 0.05$; #$p < 0.01$. FXR, farnesoid X receptor; LF, low-fat control diet; WD, Western diet.

Other factors such as gut microbiome, which is largely involved in host metabolism regulation, may act as additional possible contributor to our findings. As expected, WD-fed mice exhibited markedly altered gut microbiota, especially within the colon. WD-feeding was characterized by elevated colonic Bacteroidetes (*e.g.*, S24-7) and reduced Firmicutes (*e.g.*, *Allobaculum spp.* and *Christensenellaceae spp.*), compared with LF animals. However, WD-induced dysbiosis was reduced by INT-767 treatment, which prevented the changes in Bacteroidetes and Firmicutes levels observed in the untreated WD group. Although we cannot rule out a direct effect of INT-767 on the gut microbiota, INT-767 did not restore WD-induced microbial dysbiosis in *Fxr*-null mice, suggesting that host-dependent bile-acid signaling pathways are a determinant of gut microbiota composition. Overall, these results imply that changes in the gut microbiota in response to WD do not simply result from direct effects of elevated nutrient availability to resident microbial communities but that diet-

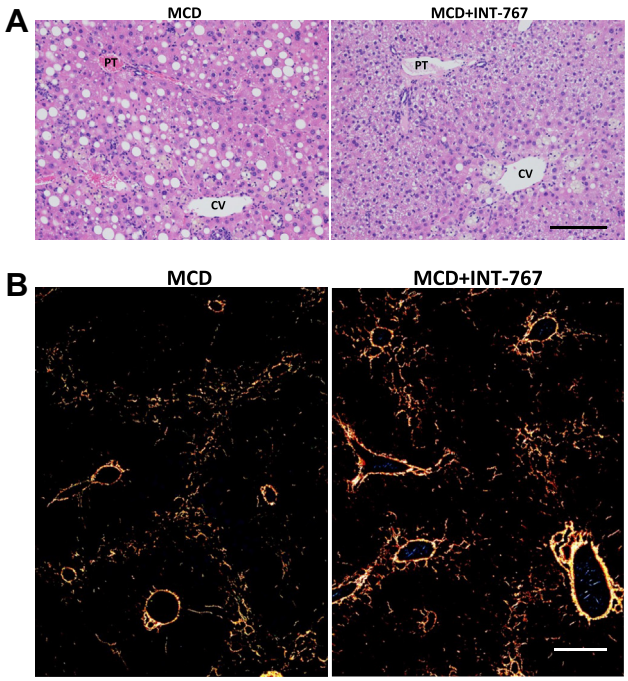

Figure 9. The effects of INT-767 on MCD induced NASH. *A*, steatosis as determined by H&E staining; *B*, fibrosis as determined by Picro-Sirius Red staining. Size bars = 100 microns. H&E, hematoxylin and eosin; MCD, methionine and choline–deficient diet; NASH, nonalcoholic steatohepatitis.

induced functional modification(s) of the gut–liver axis play a larger role in determining microbiome composition and function.

In our study, we also explored the FXR-dependent mechanisms lowering hepatic lipids. We found that INT-767 markedly inhibits expression of hepatic Cyp7a1 and Cyp8b1, two major enzymes involved in bile acid synthesis. This led to decreased total bile acid content and caused marked modifications in liver and intestinal bile acid composition with decreased hydrophobicity index, known to inhibit intestinal cholesterol absorption (33). INT-767-induced FXR activation prevented SREBP-1c-, ChREBPα-, and ChREBPβ-mediated fatty acid synthesis, CD36- and FABP1-mediated fatty acid uptake, and LOX-1-mediated cholesterol uptake in the liver. LXRα may be also involved, as lowering cholesterol can decrease LXRα activity, which in turn reduce its target SREBP-1c expression. INT-767 activates FXR in both liver and intestine, in contrast with the findings that intestinal FXR inhibition is beneficial in preventing NASH (46). While we expect data from tissue-specific FXR knockout mice to provide a more specific direction, we speculate that intestinal FXR is dispensable for INT-767 function, as one of bile acid synthesis enzymes, Cyp8b1, does not require intestinal FXR (33).

In addition, INT-767 increased p-AMPK, SIRT1, PGC-1α, and SIRT3, which are master regulators of mitochondrial biogenesis and mitochondrial function. Despite no changes in mitochondrial DNA/nuclear DNA ratio, INT-767 improved mitochondrial function, as evidenced by the near reversal of WD-induced decrease in complex I activity and a significant increase in complex IV activity. Recent studies indicate that improving mitochondrial function per se may mediate anti-inflammatory, antioxidative, and antifibrotic effects (47–50).

The anti2-fibrotic effects of INT-767 may depend on the trigger of fibrosis in each model. In the MCD-induced NASH model, we observed a different effect with INT-767. It is known that MCD-induced liver fibrosis is independent of steatosis (34). In our study, although steatosis was almost completely prevented by INT-767, MCD-induced liver fibrosis still progressed in the presence of INT-767, unlike WD-induced NASH, suggesting that its antifibrotic effects depend on specific mechanisms of fibrosis development in each model.

In summary, the present results indicate that WD in C57BL/6J mice induces steatosis, inflammation, and fibrosis (NASH), associated with mitochondrial dysfunction and gut microbiota dysbiosis. Prevention or treatment with the dual FXR-TGR5 agonist INT-767 can arrest the progression of WD-induced NASH in mice, mediated largely by FXR-dependent, TGR5-independent mechanisms.

Experimental procedures

Liver biopsy samples from human subjects

We obtained deidentified liver biopsy samples (FFPE) from the pathological archives at the University of Colorado. These samples were from healthy donors as well as subjects with stage 0 to 4 liver fibrosis, as scored blindly by the liver pathologist (D.E.K.) based on the Brunt and Kleiner scoring systems (51, 52). The samples were stained with H&E, Masson's trichrome, and imaged by two-photon excitation–second harmonic generation microscopy for label-free imaging of fibrosis. We also performed immunohistochemistry for FXR and TGR5 expression in the liver samples.

TGR5 and FXR immunohistochemistry

Briefly, staining was performed on 5 um formalin-fixed paraffin-embedded sections with anti-TGR5 rabbit polyclonal antibody (1:200 for 2 h; Sigma-Aldrich, product number HPA062890) or anti-FXR monoclonal antibody (R&D, product number PP-A9033A-00). Image analysis was performed using ImageScope (Leica Biosystems Pathology Imaging) with positive pixel count algorithms for TGR5 staining and nuclear algorithm for FXR staining.

Animal models

The mouse studies were performed with wildtype C57BL6/J, FXR knockout (*Fxr*-null) male mice on the C57BL6/J background obtained from Jackson Laboratories and *TGR5*-null mice backcrossed to the C57BL6/J background (a gift from Professor Johan Auwerx, École Polytechnique Fédérale de Lausanne, Switzerland). The mice were housed four mice per cage, kept at room temperature using a 12-h dark to 12-h light cycle, and allowed free access to food and water.

For the intervention study, 8-week-old male C57BL/6J mice were fed a WD consisting of 42 kcal % milkfat, 42.7 kcal % carbohydrate, 15.2 kcal % protein, and supplemented with 0.2% cholesterol (Harlan Teklad TD.88137) or a LF consisting

of 13 kcal % fat, 67.9 kcal % carbohydrates, and 19.1 kcal % protein, without added cholesterol (Harlan Teklad TD.08485) for 3 months to induce liver injury, at which time the mice were maintained on the same diets without supplementation or were fed the same diets supplemented with 30 mg/kg body weight INT-767 (20) for an additional 3 months. The mice were evaluated at 8 months of age, at the end of the 6-months treatment period.

To determine the role of FXR signaling in response to INT-767 treatment, wildtype 8-week-old male C57BL/6J mice and age/gender-matched *Fxr*-null mice (53) with the C57BL/6J background were fed WD, with or without supplementation with 30 mg/kg body weight INT-767, for 5 months. These mice were evaluated at 7 months of age, at the end of the 5-months treatment period.

To determine the role of TGR5 signaling in response to INT-767 treatment, we used 8-week-old male *TGR5*-null mice fed WD with or without supplementation with 30 mg/kg body weight INT-767. These mice were evaluated at 8 months of age, at the end of the 6-month treatment period.

To compare the effects of different agonists, 8-week-old male C57BL/6J mice were fed WD alone or WD supplemented with INT-767 or INT-747 (Intercept) or INT-777 (Intercept) at 30 mg/kg body weight for 6 months.

To determine if INT-767 was also effective in a different NASH model, eight-week-old male C57BL/6J mice were fed a MCD (Research Diets A02082002B) with or without 30 mg/kg body weight INT-767 for 12 weeks.

At the end of the treatment periods, the mice were anesthetized, blood (serum) was obtained from the vena cava, and then the liver and intestine were harvested and processed for the biochemical and imaging studies detailed below.

Blood chemistry

Blood glucose levels were measured with a Glucometer Elite XL (Bayer). Plasma triglyceride and cholesterol were measured with kits from Wako Chemical. Plasma liver enzymes were analyzed with kits from Bioassay Systems.

RNA extraction and real-time quantitative PCR

Total RNA was isolated from the livers using Qiagen RNeasy mini kit, and cDNA was synthesized using reverse transcript reagents from Bio-Rad Laboratories. Quantitative real-time PCR was performed as previously described (54–57), and expression levels of target genes were normalized to 18S level. Primer sequences are listed in Table S2.

Western blotting

Western blotting was performed as previously described (54–57). An equal amount of total protein was separated by SDS-PAGE gels and transferred onto PVDF membranes. After HRP-conjugated secondary antibodies, the immune complexes were detected by chemiluminescence captured on UVP Biospectrum 500 Imaging System, and the densitometry was performed with ImageJ software. Antibodies against AMPK (07-350, Millipore), sirtuin 1 (05-1243, Millipore), PGC-1α (AB3242, Millipore), p-AMPK (Thr172, 2531, Cell Signaling), sirtuin 3 (5490, Cell Signaling), and SOD2 (ADI-SOD-110, Enzo Life Sciences) were used for Western blotting.

Autofluorescence FLIM, SHG, and THG measurements using DIVER microscope

To determine the effects of WD and treatment with INT-767 on lipids and fibrillary collagens, autofluorescence FLIM, SHG, and THG signals were acquired using the DIVER microscope developed at the Laboratory for Fluorescence Dynamics, University of California at Irvine, CA, as detailed in Supplementary Methods.

Histological stains and assessment

Paraffin sections (5 μm) were used for histological stains. H&E stained sections were scored for liver injury according to the liver scoring system similar to that of Kleiner *et al.* (52) but modified for mouse liver (31). For quantification of the fibrosis following picrosirius red (PSR) staining, ten polarized light images were made in a "tiling" fashion across each PSR stained slide and then quantified using the 3I Slidebook program (3I) to arrive at the PSR positive pixels per 100× field for that slide. Immunofluorescent staining was performed for Perilipin 2 (20R-AP002, Fitzgerald Industries), CD3epsilon, collagen type 1, and collagen type 3, all as previously described (58) with detection using secondary antibodies conjugated with Alexafluor 488 or Alexafluor 594 at dilutions of 1:500 and 1:250, respectively and nuclear staining with DAPI (4′, 6-diamidino-2-phenylindole, Sigma Chemical Co). Immunofluorescence images were captured on a Nikon Diaphot fluorescence microscope and digitally deconvolved using the No Neighbors algorithm (Slidebook) as described previously (59).

Mouse collagen mass spectroscopy

Tryptic digests of mouse liver samples were analyzed by LC-MS/MS using multiple reaction monitoring targeted mass spectrometry on a triple quadrupole mass spectrometer, as detailed in Supplementary Methods and Table S3.

Hepatic triglyceride and cholesterol concentration and lipidomics

Total hepatic triglyceride and cholesterol levels were quantified as described previously (60) and as detailed in Supplementary Methods.

Serum, liver, and intestine bile acid composition analysis

Concentrations of bile acids were determined by an Acquity UPLC/Xevo G2 QTOFMS system (Waters Corp.) with an ESI source. An Acquity BEH C18 column (100 × 2.1 mm internal diameter, 1.7 mm, Waters Corp.) was applied for chromatographic separation. A mixture of 0.1% formic acid in water (A) and 0.1% formic acid in acetonitrile (B) was used as the mobile phase. The gradient elution was started from 80% (A) for 4 min, decreased linearly to 60% (A) over 11 min, to 40% (A) over the next 5 min, to 10% (A) for the succeeding 1 min, and

finally increased to 80% (A) for 4 min to re-equilibrate the column. The column temperature was maintained at 45 °C, and the flow rate was 0.4 ml/min. Mass spectrometry detection was operated in negative mode. A mass range of m/z 50 to 850 was acquired (61, 62).

Microbiome analysis

Broad-range PCR and sequencing of 16S rRNA genes followed our previously described protocols (63, 64). In brief, DNA was extracted from 50 to 100 mg of cecal or colon contents using the QIAmp Stool DNA isolation kit (QIAGEN, Inc). 16S rRNA gene PCR amplicons were generated using barcoded primers (65) targeting the V3V4 variable region: primers 338F (5′ ACTCCTACGGGAGGCAGCAG) and 806R (5′ GGACTACHVGGGTWTCTAAT) (66, 67). Sequencing was performed on the Illumina MiSeq platform using a 600-cycle version 3 reagent kit, version v2.3.0.8 of the MiSeq Control Software, and version v2.3.32 of MiSeq Reporter. Demultiplexed paired-end reads were assembled using phrap (68) and pairs that did not assemble were discarded. Potential chimeras were identified and discarded using UCHIME (usearch6.0.203_i86linux32) (69) and the Schloss (70) Silva reference sequences. Assembled sequences were aligned and classified with SINA (1.3.0-r23838) (71) using the Silva 115NR99 database (72) as the reference. Operational taxonomic units were produced by clustering sequences with identical taxonomic assignments.

Statistical analysis

Results are presented as the means ± SEM for at least three independent experiments. Data were analyzed by ANOVA and Student–Newman–Keuls tests for multiple comparisons or by *t* test for unpaired data between two groups (GraphPad Prism). Statistical significance was accepted at the $p < 0.05$ level. Microbiome analyses used Explicet (73) and the R statistical software package (74). The relative abundance of each taxon was calculated as the number of 16S rRNA sequences of a given taxon divided by the total number of 16S rRNA sequences in a patient's sample. Differences in overall microbiome composition (*i.e.*, beta-diversity) between subsets were assessed by nonparametric multivariate analysis of variance test using Morisita-Horn dissimilarities; *p*-values were estimated through 1,000,000 permutations. Shannon diversity, Shannon evenness, and richness (Sobs) were calculated using rarefaction and compared across groups through ANOVA tests. Comparisons of relative abundance across groups were conducted by nonparametric Kruskal-Wallis tests. Associations between cecal bile acid species concentrations and relative abundances of genus-level bacterial taxa were assessed by Spearman rank-sum correlation tests.

Study approval

Animal studies and relative protocols were approved by the Animal Care and Use Committee at the University of Colorado AMC, Aurora, Colorado, and Georgetown University, Washington, DC. All animal experimentation was conducted in accordance with the Guide for Care and Use of Laboratory Animals (National Institutes of Health, Bethesda, MD).

Data availability

All the data described in the article are located within the article and/or its supporting information.

Supporting information—This article contains supporting information.

Author contributions—M. L. and X. X. W. conceptualization; M. L. and X. X. W. methodology; X. X. W., C. X., A. E. L., S. R., J. L., K. M., K. B., D. J. O., S. T., A. D., D. E. K., S. M. H., K. W. K., A. R., C. E. R., Y. L. and D. I. investigation; X. X. W., D. J. O., and D. N. F. formal analysis; X. X. W., D. J. O., and D. N. F. data curation; X. X. W. writing-original draft; B. A. J., L. A., J. B. K., J. L. M., F. J. G., E. G., and M. L. writing-review and editing.

Funding and additional information—These studies were supported by grant support from National Institutes of Health (NIH) R01 AG049493 and DK116567 (M. L.), NIH NIGMS P41-GM103540 (E. G. and S. R.), Medical School Grant by Intercept (M. L., X. X. W. and S. R.), NIH TL1 TR001431 and F30 DK129003 (B. A. J.), AHA Fellowship Grants (A. E. L. and K. M.), Intramural Program of NIDDK (J. B. K., A. R., and J. L.), and NCI (F. J. G., K. W. K., S. M. H., and D. E. K.). The content is solely the responsibility of the authors and does not necessarily represent the official views of the National Institutes of Health.

Conflict of interest—Dr Luciano Adorini is an employee of Intercept. These studies were in part supported by a medical school Investigator Initiated Study (IIS) grant to Moshe Levi. The authors otherwise have no other conflict of interest.

Abbreviations—The abbreviations used are: FLIM, fluorescence lifetime imaging microscopy; FXR, farnesoid X receptor; LF, low-fat control diet; MCD, methionine and choline–deficient diet; NAFLD, nonalcoholic fatty liver disease; NASH, nonalcoholic steatohepatitis; OCA, obeticholic acid; SHG, second harmonic generation; THG, third harmonic generation; WD, Western diet.

References

1. Levene, A. P., and Goldin, R. D. (2012) The epidemiology, pathogenesis and histopathology of fatty liver disease. *Histopathology* **61**, 141–152
2. Spengler, E. K., and Loomba, R. (2015) Recommendations for diagnosis, referral for liver biopsy, and treatment of nonalcoholic fatty liver disease and nonalcoholic steatohepatitis. *Mayo Clin. Proc.* **90**, 1233–1246
3. Wree, A., Broderick, L., Canbay, A., Hoffman, H. M., and Feldstein, A. E. (2013) From NAFLD to NASH to cirrhosis-new insights into disease mechanisms. *Nat. Rev. Gastroenterol. Hepatol.* **10**, 627–636
4. Stal, P. (2015) Liver fibrosis in non-alcoholic fatty liver disease - diagnostic challenge with prognostic significance. *World J. Gastroenterol.* **21**, 11077–11087
5. Marchesini, G., Petta, S., and Dalle Grave, R. (2016) Diet, weight loss, and liver health in nonalcoholic fatty liver disease: pathophysiology, evidence, and practice. *Hepatology* **63**, 2032–2043
6. Corey, K. E., and Rinella, M. E. (2016) Medical and surgical treatment options for nonalcoholic steatohepatitis. *Dig. Dis. Sci.* **61**, 1387–1397

7. Brodosi, L., Marchignoli, F., Petroni, M. L., and Marchesini, G. (2016) NASH: a glance at the landscape of pharmacological treatment. *Ann. Hepatol.* **15**, 673–681
8. Kohli, R., Myronovych, A., Tan, B. K., Salazar-Gonzalez, R. M., Miles, L., Zhang, W., *et al.* (2015) Bile acid signaling: mechanism for bariatric surgery, cure for NASH? *Dig. Dis.* **33**, 440–446
9. Mintziori, G., and Polyzos, S. A. (2016) Emerging and future therapies for nonalcoholic steatohepatitis in adults. *Expert Opin. Pharmacother.* **17**, 1937–1946
10. Mudaliar, S., Henry, R. R., Sanyal, A. J., Morrow, L., Marschall, H. U., Kipnes, M., *et al.* (2013) Efficacy and safety of the farnesoid X receptor agonist obeticholic acid in patients with type 2 diabetes and nonalcoholic fatty liver disease. *Gastroenterology* **145**, 574–582.e1
11. Morrison, M. C., Verschuren, L., Salic, K., Verheij, J., Menke, A., Wielinga, P. Y., *et al.* (2018) Obeticholic acid modulates serum metabolites and gene signatures characteristic of human NASH and attenuates inflammation and fibrosis progression in Ldlr-/-.Leiden mice. *Hepatol. Commun.* **2**, 1513–1532
12. Younossi, Z. M., Ratziu, V., Loomba, R., Rinella, M., Anstee, Q. M., Goodman, Z., *et al.* (2019) Obeticholic acid for the treatment of non-alcoholic steatohepatitis: interim analysis from a multicentre, randomised, placebo-controlled phase 3 trial. *Lancet* **394**, 2184–2196
13. Myronovych, A., Kirby, M., Ryan, K. K., Zhang, W., Jha, P., Setchell, K. D., *et al.* (2014) Vertical sleeve gastrectomy reduces hepatic steatosis while increasing serum bile acids in a weight-loss-independent manner. *Obesity (Silver Spring)* **22**, 390–400
14. Ryan, K. K., Tremaroli, V., Clemmensen, C., Kovatcheva-Datchary, P., Myronovych, A., Karns, R., *et al.* (2014) FXR is a molecular target for the effects of vertical sleeve gastrectomy. *Nature* **509**, 183–188
15. Ding, L., Sousa, K. M., Jin, L., Dong, B., Kim, B. W., Ramirez, R., *et al.* (2016) Vertical sleeve gastrectomy activates GPBAR-1/TGR5 to sustain weight loss, improve fatty liver, and remit insulin resistance in mice. *Hepatology* **64**, 760–773
16. Kawamata, Y., Fujii, R., Hosoya, M., Harada, M., Yoshida, H., Miwa, M., *et al.* (2003) A G protein-coupled receptor responsive to bile acids. *J. Biol. Chem.* **278**, 9435–9440
17. Maruyama, T., Miyamoto, Y., Nakamura, T., Tamai, Y., Okada, H., Sugiyama, E., *et al.* (2002) Identification of membrane-type receptor for bile acids (M-BAR). *Biochem. Biophys. Res. Commun.* **298**, 714–719
18. Chiang, J. Y. (2013) Bile acid metabolism and signaling. *Compr. Physiol.* **3**, 1191–1212
19. Thomas, C., Gioiello, A., Noriega, L., Strehle, A., Oury, J., Rizzo, G., *et al.* (2009) TGR5-mediated bile acid sensing controls glucose homeostasis. *Cell Metab.* **10**, 167–177
20. Rizzo, G., Passeri, D., De Franco, F., Ciaccioli, G., Donadio, L., Rizzo, G., *et al.* (2010) Functional characterization of the semisynthetic bile acid derivative INT-767, a dual farnesoid X receptor and TGR5 agonist. *Mol. Pharmacol.* **78**, 617–630
21. Jadhav, K., Xu, Y., Xu, Y., Li, Y., Xu, J., Zhu, Y., *et al.* (2018) Reversal of metabolic disorders by pharmacological activation of bile acid receptors TGR5 and FXR. *Mol. Metab.* **9**, 131–140
22. Baandrup Kristiansen, M. N., Veidal, S. S., Christoffersen, C., Feigh, M., Vrang, N., Roth, J. D., *et al.* (2019) Validity of biopsy-based drug effects in a diet-induced obese mouse model of biopsy-confirmed NASH. *BMC Gastroenterol.* **19**, 228
23. Hu, Y. B., Liu, X. Y., and Zhan, W. (2018) Farnesoid X receptor agonist INT-767 attenuates liver steatosis and inflammation in rat model of nonalcoholic steatohepatitis. *Drug Des. Dev. Ther.* **12**, 2213–2221
24. Comeglio, P., Cellai, I., Mello, T., Filippi, S., Maneschi, E., Corcetto, F., *et al.* (2018) INT-767 prevents NASH and promotes visceral fat brown adipogenesis and mitochondrial function. *J. Endocrinol.* **238**, 107–127
25. Roth, J. D., Feigh, M., Veidal, S. S., Fensholdt, L. K., Rigbolt, K. T., Hansen, H. H., *et al.* (2018) INT-767 improves histopathological features in a diet-induced ob/ob mouse model of biopsy-confirmed non-alcoholic steatohepatitis. *World J. Gastroenterol.* **24**, 195–210
26. McMahan, R. H., Wang, X. X., Cheng, L. L., Krisko, T., Smith, M., El Kasmi, K., *et al.* (2013) Bile acid receptor activation modulates hepatic monocyte activity and improves nonalcoholic fatty liver disease. *J. Biol. Chem.* **288**, 11761–11770
27. Pathak, P., Liu, H., Boehme, S., Xie, C., Krausz, K. W., Gonzalez, F., *et al.* (2017) Farnesoid X receptor induces Takeda G-protein receptor 5 cross-talk to regulate bile acid synthesis and hepatic metabolism. *J. Biol. Chem.* **292**, 11055–11069
28. Arab, J. P., Karpen, S. J., Dawson, P. A., Arrese, M., and Trauner, M. (2017) Bile acids and nonalcoholic fatty liver disease: molecular insights and therapeutic perspectives. *Hepatology* **65**, 350–362
29. Trauner, M., Fuchs, C. D., Halilbasic, E., and Paumgartner, G. (2017) New therapeutic concepts in bile acid transport and signaling for management of cholestasis. *Hepatology* **65**, 1393–1404
30. Stephenson, K., Kennedy, L., Hargrove, L., Demieville, J., Thomson, J., Alpini, G., *et al.* (2018) Updates on dietary models of nonalcoholic fatty liver disease: current studies and insights. *Gene Expr.* **18**, 5–17
31. Lanaspa, M. A., Andres-Hernando, A., Orlicky, D. J., Cicerchi, C., Jang, C., Li, N., *et al.* (2018) Ketohexokinase C blockade ameliorates fructose-induced metabolic dysfunction in fructose-sensitive mice. *J. Clin. Invest.* **128**, 2226–2238
32. Kisseleva, T. (2017) The origin of fibrogenic myofibroblasts in fibrotic liver. *Hepatology* **65**, 1039–1043
33. Xu, Y., Li, F., Zalzala, M., Xu, J., Gonzalez, F. J., Adorini, L., *et al.* (2016) Farnesoid X receptor activation increases reverse cholesterol transport by modulating bile acid composition and cholesterol absorption in mice. *Hepatology* **64**, 1072–1085
34. Itagaki, H., Shimizu, K., Morikawa, S., Ogawa, K., and Ezaki, T. (2013) Morphological and functional characterization of non-alcoholic fatty liver disease induced by a methionine-choline-deficient diet in C57BL/6 mice. *Int. J. Clin. Exp. Pathol.* **6**, 2683–2696
35. Iracheta-Vellve, A., Calenda, C. D., Petrasek, J., Ambade, A., Kodys, K., Adorini, L., *et al.* (2018) FXR and TGR5 agonists ameliorate liver injury, steatosis, and inflammation after binge or prolonged alcohol feeding in mice. *Hepatol. Commun.* **2**, 1379–1391
36. Dvornikov, A., and Gratton, E. (2016) Imaging in turbid media: a transmission detector gives 2-3 order of magnitude enhanced sensitivity compared to epi-detection schemes. *Biomed. Opt. Express* **7**, 3747–3755
37. Ranjit, S., Dobrinskikh, E., Montford, J., Dvornikov, A., Lehman, A., Orlicky, D. J., *et al.* (2016) Label-free fluorescence lifetime and second harmonic generation imaging microscopy improves quantification of experimental renal fibrosis. *Kidney Int.* **90**, 1123–1128
38. Ranjit, S., Dvornikov, A., Dobrinskikh, E., Wang, X., Luo, Y., Levi, M., *et al.* (2017) Measuring the effect of a Western diet on liver tissue architecture by FLIM autofluorescence and harmonic generation microscopy. *Biomed. Opt. Express* **8**, 3143–3154
39. Verbeke, L., Mannaerts, I., Schierwagen, R., Govaere, O., Klein, S., Vander Elst, I., *et al.* (2016) FXR agonist obeticholic acid reduces hepatic inflammation and fibrosis in a rat model of toxic cirrhosis. *Sci. Rep.* **6**, 33453
40. Ding, Z. M., Xiao, Y., Wu, X., Zou, H., Yang, S., Shen, Y., *et al.* (2018) Progression and regression of hepatic lesions in a mouse model of NASH induced by dietary intervention and its implications in pharmacotherapy. *Front. Pharmacol.* **9**, 410
41. Ganz, M., Bukong, T. N., Csak, T., Saha, B., Park, J. K., Ambade, A., *et al.* (2015) Progression of non-alcoholic steatosis to steatohepatitis and fibrosis parallels cumulative accumulation of danger signals that promote inflammation and liver tumors in a high fat-cholesterol-sugar diet model in mice. *J. Transl. Med.* **13**, 193
42. Vassileva, G., Hu, W., Hoos, L., Tetzloff, G., Yang, S., Liu, L., *et al.* (2010) Gender-dependent effect of Gpbar1 genetic deletion on the metabolic profiles of diet-induced obese mice. *J. Endocrinol.* **205**, 225–232
43. Pols, T. W., Noriega, L. G., Nomura, M., Auwerx, J., and Schoonjans, K. (2011) The bile acid membrane receptor TGR5 as an emerging target in metabolism and inflammation. *J. Hepatol.* **54**, 1263–1272
44. Donepudi, A. C., Boehme, S., Li, F., and Chiang, J. Y. (2017) G-protein-coupled bile acid receptor plays a key role in bile acid metabolism and fasting-induced hepatic steatosis in mice. *Hepatology* **65**, 813–827
45. Chiang, J. Y. L., and Ferrell, J. M. (2018) Bile acid metabolism in liver pathobiology. *Gene Expr.* **18**, 71–87

46. Jiang, C., Xie, C., Lv, Y., Li, J., Krausz, K. W., Shi, J., *et al.* (2015) Intestine-selective farnesoid X receptor inhibition improves obesity-related metabolic dysfunction. *Nat. Commun.* **6**, 10166
47. Gariani, K., Menzies, K. J., Ryu, D., Wegner, C. J., Wang, X., Ropelle, E. R., *et al.* (2016) Eliciting the mitochondrial unfolded protein response by nicotinamide adenine dinucleotide repletion reverses fatty liver disease in mice. *Hepatology* **63**, 1190–1204
48. Gariani, K., Ryu, D., Menzies, K. J., Yi, H. S., Stein, S., Zhang, H., *et al.* (2017) Inhibiting poly ADP-ribosylation increases fatty acid oxidation and protects against fatty liver disease. *J. Hepatol.* **66**, 132–141
49. Ryu, D., Zhang, H., Ropelle, E. R., Sorrentino, V., Mazala, D. A., Mouchiroud, L., *et al.* (2016) NAD+ repletion improves muscle function in muscular dystrophy and counters global PARylation. *Sci. Transl. Med.* **8**, 361ra139
50. Mukhopadhyay, P., Horvath, B., Rajesh, M., Varga, Z. V., Gariani, K., Ryu, D., *et al.* (2017) PARP inhibition protects against alcoholic and non-alcoholic steatohepatitis. *J. Hepatol.* **66**, 589–600
51. Brunt, E. M., Janney, C. G., Di Bisceglie, A. M., Neuschwander-Tetri, B. A., and Bacon, B. R. (1999) Nonalcoholic steatohepatitis: a proposal for grading and staging the histological lesions. *Am. J. Gastroenterol.* **94**, 2467–2474
52. Kleiner, D. E., Brunt, E. M., Van Natta, M., Behling, C., Contos, M. J., Cummings, O. W., *et al.* (2005) Design and validation of a histological scoring system for nonalcoholic fatty liver disease. *Hepatology* **41**, 1313–1321
53. Sinal, C. J., Tohkin, M., Miyata, M., Ward, J. M., Lambert, G., and Gonzalez, F. J. (2000) Targeted disruption of the nuclear receptor FXR/BAR impairs bile acid and lipid homeostasis. *Cell* **102**, 731–744
54. Jiang, T., Wang, X. X., Scherzer, P., Wilson, P., Tallman, J., Takahashi, H., *et al.* (2007) Farnesoid X receptor modulates renal lipid metabolism, fibrosis, and diabetic nephropathy. *Diabetes* **56**, 2485–2493
55. Wang, X. X., Jiang, T., Shen, Y., Caldas, Y., Miyazaki-Anzai, S., Santamaria, H., *et al.* (2010) Diabetic nephropathy is accelerated by farnesoid X receptor deficiency and inhibited by farnesoid X receptor activation in a type 1 diabetes model. *Diabetes* **59**, 2916–2927
56. Wang, X. X., Edelstein, M. H., Gafter, U., Qiu, L., Luo, Y., Dobrinskikh, E., *et al.* (2016) G protein-coupled bile acid receptor TGR5 activation inhibits kidney disease in obesity and diabetes. *J. Am. Soc. Nephrol.* **27**, 1362–1378
57. Wang, X. X., Jiang, T., Shen, Y., Adorini, L., Pruzanski, M., Gonzalez, F. J., *et al.* (2009) The farnesoid X receptor modulates renal lipid metabolism and diet-induced renal inflammation, fibrosis, and proteinuria. *Am. J. Physiol. Renal Physiol.* **297**, F1587–F1596
58. Orlicky, D. J., Libby, A. E., Bales, E. S., McMahan, R. H., Monks, J., La Rosa, F. G., *et al.* (2019) Perilipin-2 promotes obesity and progressive fatty liver disease in mice through mechanistically distinct hepatocyte and extra-hepatocyte actions. *J. Physiol.* **597**, 1565–1584
59. Russell, T. D., Palmer, C. A., Orlicky, D. J., Fischer, A., Rudolph, M. C., Neville, M. C., *et al.* (2007) Cytoplasmic lipid droplet accumulation in developing mammary epithelial cells: roles of adipophilin and lipid metabolism. *J. Lipid Res.* **48**, 1463–1475
60. Libby, A. E., Bales, E., Orlicky, D. J., and McManaman, J. L. (2016) Perilipin-2 deletion impairs hepatic lipid accumulation by interfering with sterol regulatory element-binding protein (SREBP) activation and altering the hepatic lipidome. *J. Biol. Chem.* **291**, 24231–24246
61. Xie, C., Jiang, C., Shi, J., Gao, X., Sun, D., Sun, L., *et al.* (2017) An intestinal farnesoid X receptor-ceramide signaling axis modulates hepatic gluconeogenesis in mice. *Diabetes* **66**, 613–626
62. Jiang, C., Xie, C., Li, F., Zhang, L., Nichols, R. G., Krausz, K. W., *et al.* (2015) Intestinal farnesoid X receptor signaling promotes nonalcoholic fatty liver disease. *J. Clin. Invest.* **125**, 386–402
63. Jobira, B., Frank, D. N., Pyle, L., Silveira, L. J., Kelsey, M. M., Garcia-Reyes, Y., *et al.* (2020) Obese adolescents with PCOS have altered biodiversity and relative abundance in gastrointestinal microbiota. *J. Clin. Endocrinol. Metab.* **105**, e2134–e2144
64. MacLaren, R., Radcliffe, R. A., Van Matre, E. T., Robertson, C. E., Ir, D., and Frank, D. N. (2019) The acute influence of acid suppression with esomeprazole on gastrointestinal microbiota and brain gene expression profiles in a murine model of restraint stress. *Neuroscience* **398**, 206–217
65. Frank, D. N. (2009) BARCRAWL and BARTAB: software tools for the design and implementation of barcoded primers for highly multiplexed DNA sequencing. *BMC Bioinformatics* **10**, 362
66. Lane, D. J., Pace, B., Olsen, G. J., Stahl, D. A., Sogin, M. L., and Pace, N. R. (1985) Rapid determination of 16S ribosomal RNA sequences for phylogenetic analyses. *Proc. Natl. Acad. Sci. U. S. A.* **82**, 6955–6959
67. Weisburg, W. G., Barns, S. M., Pelletier, D. A., and Lane, D. J. (1991) 16S ribosomal DNA amplification for phylogenetic study. *J. Bacteriol.* **173**, 697–703
68. Ewing, B., and Green, P. (1998) Base-calling of automated sequencer traces using phred. II. Error probabilities. *Genome Res.* **8**, 186–194
69. Edgar, R. C., Haas, B. J., Clemente, J. C., Quince, C., and Knight, R. (2011) UCHIME improves sensitivity and speed of chimera detection. *Bioinformatics* **27**, 2194–2200
70. Schloss, P. D., and Westcott, S. L. (2011) Assessing and improving methods used in operational taxonomic unit-based approaches for 16S rRNA gene sequence analysis. *Appl. Environ. Microbiol.* **77**, 3219–3226
71. Pruesse, E., Peplies, J., and Glockner, F. O. (2012) SINA: accurate high-throughput multiple sequence alignment of ribosomal RNA genes. *Bioinformatics* **28**, 1823–1829
72. Quast, C., Pruesse, E., Yilmaz, P., Gerken, J., Schweer, T., Yarza, P., *et al.* (2013) The SILVA ribosomal RNA gene database project: improved data processing and web-based tools. *Nucleic Acids Res.* **41**, D590–D596
73. Robertson, C. E., Harris, J. K., Wagner, B. D., Granger, D., Browne, K., Tatem, B., *et al.* (2013) Explicet: graphical user interface software for metadata-driven management, analysis and visualization of microbiome data. *Bioinformatics* **29**, 3100–3101
74. R Development Core Team (2014) *R: A Language and Environment for Statistical Computing*, R Foundation for Statistical Computing, Vienna, Austria